

Reduced-cost second-order algebraic-diagrammatic construction method for excitation energies and transition moments

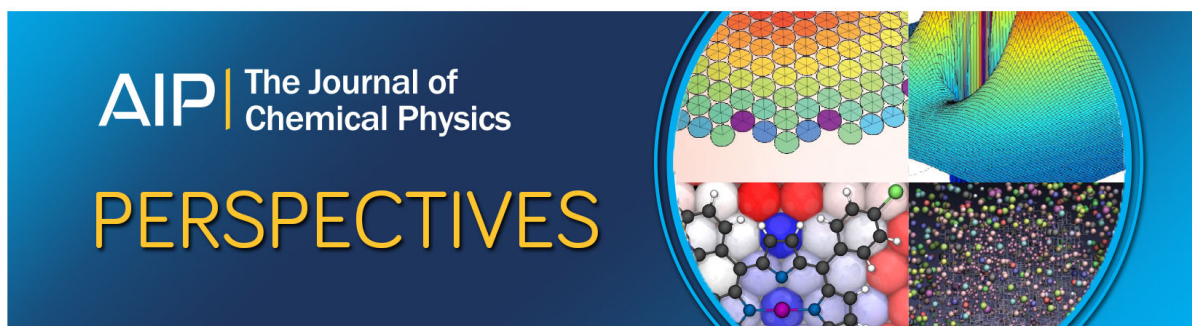
Dávid Mester, Péter R. Nagy, and Mihály Kállay

Citation: *The Journal of Chemical Physics* **148**, 094111 (2018); doi: 10.1063/1.5021832

View online: <https://doi.org/10.1063/1.5021832>

View Table of Contents: <http://aip.scitation.org/toc/jcp/148/9>

Published by the [American Institute of Physics](#)



Reduced-cost second-order algebraic-diagrammatic construction method for excitation energies and transition moments

Dávid Mester,^{a)} Péter R. Nagy, and Mihály Kállay^{b)}

MTA-BME Lendület Quantum Chemistry Research Group, Department of Physical Chemistry and Materials Science, Budapest University of Technology and Economics, P.O. Box 91, H-1521 Budapest, Hungary

(Received 9 January 2018; accepted 19 February 2018; published online 7 March 2018)

A reduced-cost implementation of the second-order algebraic-diagrammatic construction [ADC(2)] method is presented. We introduce approximations by restricting virtual natural orbitals and natural auxiliary functions, which results, on average, in more than an order of magnitude speedup compared to conventional, density-fitting ADC(2) algorithms. The present scheme is the successor of our previous approach [D. Mester, P. R. Nagy, and M. Kállay, *J. Chem. Phys.* **146**, 194102 (2017)], which has been successfully applied to obtain singlet excitation energies with the linear-response second-order coupled-cluster singles and doubles model. Here we report further methodological improvements and the extension of the method to compute singlet and triplet ADC(2) excitation energies and transition moments. The various approximations are carefully benchmarked, and conservative truncation thresholds are selected which guarantee errors much smaller than the intrinsic error of the ADC(2) method. Using the canonical values as reference, we find that the mean absolute error for both singlet and triplet ADC(2) excitation energies is 0.02 eV, while that for oscillator strengths is 0.001 a.u. The rigorous cutoff parameters together with the significantly reduced operation count and storage requirements allow us to obtain accurate ADC(2) excitation energies and transition properties using triple- ζ basis sets for systems of up to one hundred atoms. *Published by AIP Publishing.* <https://doi.org/10.1063/1.5021832>

I. INTRODUCTION

There are several, nowadays, actively researched phenomena related to the excited electronic states of molecular systems. For instance, excited states play an important role for photochromic materials, for photo-initialized chemical processes, and for energy transfer and storage. Quantum-chemical methods have now become routine tools in the investigation of excited-state properties and processes. Consequently, it is important to develop efficient but reliable methods for the excited states of extended molecular systems.

Many theories have been developed in the past few decades to investigate excited-state and transition properties. These are, for example, the time-dependent density functional theory (TD-DFT)^{1,2} as well as the wave function-based semi-empirical^{3–6} and *ab initio* methods.^{7–27} Presently, for the investigation of extended systems with more than 1500 basis functions, a TD-DFT approach is the most common choice. However, the limits of TD-DFT have been identified previously for challenging cases,^{28,29} such as Rydberg and charge transfer (CT) states, or $\pi \rightarrow \pi^*$ excitations of a conjugated system. The correlated wave function methods usually provide a more reliable option for small cases. Excited states can simply be treated by the multi-configurational

self-consistent field (MCSCF)³⁰ method, by the multi-reference configuration interaction,³¹ or with the various propagator-based schemes.^{13,14} Excited-state theories have also been developed for coupled-cluster (CC) approaches invoking the equation-of-motion (EOM)^{7,8} and the linear-response (LR)^{9–11} techniques. However, the much higher computational demand of such methods is often a limiting factor in practice. Some of the most affordable methods, such as the complete active space SCF (CASSCF)¹⁵ approach, the second-order CC singles and doubles (CC2) method,^{16–21} the second-order polarization propagator approximation (SOPPA)^{22–24} method, and the second-order algebraic-diagrammatic construction [ADC(2)]²⁵ approach have already been applied to realistic, but relatively small systems.

Among the theories suitable for excited-state property calculations, ADC is one of the most promising approaches. It is a Hermitian and size-consistent method, and it is relatively easy to implement. The ADC scheme was first derived by Schirmer²⁵ employing a diagrammatic perturbation expansion of the polarization propagator, utilizing the Møller–Plesset partitioning of the Hamiltonian. A similar result was later obtained with the so-called intermediate state representation (ISR) approach developed by Schirmer *et al.*^{32–34} While the initial implementations of the theory were limited to its second-order variant [ADC(2)], later it was extended to the third-order [ADC(3)].^{26,27} A more efficient implementation^{35–38} of the ADC(2) and ADC(3) methods and extensive benchmark calculations³⁶ were reported by Dreuw *et al.* In these studies,

^{a)}Electronic mail: mester.david@mail.bme.hu

^{b)}Electronic mail: kallay@mail.bme.hu

the performance of ADC(2) was also compared to that of the closely related but more demanding CC2 approach, and it has been proven that the ADC(2) method is practically as accurate as CC2.^{36,39} Furthermore, tools to compute two-photon absorption,⁴⁰ static polarizability,⁴¹ core-valence excitations,⁴² and excited-state dynamics⁴³ were also developed. The ADC method was also combined with the spin-flip,⁴⁴ the scaled-opposite-spin,³⁹ and the frozen density embedding⁴⁵ approaches.

The ADC(2) method is often used to study the excited-state properties of molecular systems; however, as it scales as the fifth power of the system size, the upper limit of its applicability is around 30 heavy atoms or 1500 basis functions. For more extended systems, instead of using the less accurate TD-DFT methods, an alternative solution may be the reduction of the computational costs of the ADC(2) method. One of the most commonly used approximations for that purpose is the density fitting (DF) approach which was introduced by Shavitt *et al.*⁴⁶ and further developed by Whitten⁴⁷ and Dunlap and co-workers.⁴⁸ In the DF approach, the four-center electron repulsion integrals are written in an approximate form as the products of two- and three-center integrals; therefore, the operation count, the memory requirement, and the number of the input-output (I/O) operations can be greatly reduced.^{19,49} As it was demonstrated by Hättig, if the DF is combined with spin-scaling and Laplace transform techniques, the fifth-order scaling of ADC(2) can be reduced to fourth-order.⁵⁰ A promising new approach for the rank reduction of higher-order quantities, such as the two-electron integral or the doubles coefficient tensors, is the tensor hypercontraction (THC) scheme of Martínez, Sherrill, and their co-workers.^{51–53} It was demonstrated that the THC approach can reduce the scaling of CC2 and potentially that of ADC(2) to fourth-order even if the full exchange term is included.^{54,55}

Another widely used technique to reduce the computational costs is to restrict the subspace in which the equations are solved. One of the simplest approaches is the restricted virtual space approach, where the canonical virtual orbitals with orbital energies higher than a predetermined threshold are neglected. The method was also employed for excited-state CC models,^{56,57} while its applicability for ADC approaches was recently demonstrated by Sundholm *et al.*^{58,59} as well as Yang and Dreuw.⁶⁰ A further possibility for reducing the subspace is the introduction of local approximations used often nowadays, the basic idea of which comes from Pulay and co-workers.^{61,62} Concerning the ADC(2) method, Schütz⁶³ and Helmich and Hättig⁶⁴ developed localized molecular orbital (MO)-based approaches, while local schemes for calculating excitation energies and oscillator strengths with the related linear response (LR) CC2 method have been proposed by Schütz and co-workers^{65–70} as well as by Baudin and Kristensen.^{71,72} In the case of the frozen natural orbital (NO) approximation, a one-particle density matrix is constructed and diagonalized. Of the resulting NOs, those ones are retained which have large occupation numbers, i.e., eigenvalues, and are supposed to give a significant contribution to the electron correlation.^{73–75} While the approximation is widely used for ground-state correlation methods,^{76–79} its use for excited-state calculations are rather limited.^{80,81} A closely related

approach, the quasiparticle virtual orbital scheme, was developed by Ortiz and co-workers for the cost reduction of electron propagator methods.^{82–84} The natural auxiliary function (NAF) approach, which was introduced by one of us,⁸⁵ is similar to the NO approximation. In this case, the size of the fitting basis is reduced in a similar way as for the above-mentioned method. To the best of our knowledge, the ADC variants of the NO and NAF approximations have not been developed.

In this paper, our NO- and NAF-based approach⁸⁶ is extended to the ADC(2) method. We report an improved version of the previous algorithm which is more robust and enables significantly faster calculations. We also extend the considered excited-state properties to triplet excitation energies and transition moments. We assess the accuracy of the approach in detail and carry out calculations for organic dyes of various sizes.

II. THEORY

A. The ADC(2) method

The ground-state ADC(2) correlation energy is simply obtained from second-order Møller–Plesset (MP2) perturbation theory as

$$\Delta E_{\text{MP2}} = \sum_{ijab} (ia|jb)(2t_{ij}^{ab} - t_{ji}^{ab}), \quad (1)$$

where i, j, \dots (a, b, \dots) denote occupied (virtual) spatial molecular orbital (MO) indices. Later, p, q, \dots will be used as general MO indices. The above first-order amplitudes, t_{ij}^{ab} , are given in the canonical Hartree–Fock (HF) basis as

$$t_{ij}^{ab} = \frac{(ia|jb)}{\varepsilon_i + \varepsilon_j - \varepsilon_a - \varepsilon_b} = \frac{(ia|jb)}{D_{ij}^{ab}}, \quad (2)$$

where ε_i (ε_a) is the occupied (virtual) orbital energy and $(ia|jb)$ denotes a two-electron integral using the Mulliken notation. Utilizing this, the first-order Møller–Plesset (MP1) wave function reads as

$$|\Psi^{\text{MP1}}\rangle = (1 + T_2)|0\rangle, \quad (3)$$

where $|0\rangle$ is the HF determinant. Here the double excitations are described by T_2 in the following form:

$$T_2 = \frac{1}{2} \sum_{aibj} t_{ij}^{ab} E_{ai} E_{bj} = \frac{1}{2} \sum_{\mu_2} t_{\mu_2} \tau_{\mu_2}, \quad (4)$$

where we have introduced a shorthand notation for the excitation operator, $\tau_{\mu_2} = E_{ai} E_{bj}$, which is constructed from spin-coupled one-particle excitation operators $E_{ai} = a_{\alpha}^{\dagger} i_{\alpha}^{-} + a_{\beta}^{\dagger} i_{\beta}^{-}$ with creation operators $a_{\eta}^{\dagger}, b_{\eta}^{\dagger}, \dots$ and annihilation operators $i_{\eta}^{-}, j_{\eta}^{-}, \dots$ for spin orbitals with η spin.

The ADC(2) ansatz for the wave function of the excited states is given in the form of

$$|\Psi^{\text{ADC(2)}}\rangle = (R_1 + R_2)|\Psi^{\text{MP1}}\rangle, \quad (5)$$

where the spin-coupled single and double excitation operators, R_1 and R_2 , respectively, can be defined similar to Eq. (4) with r_{μ_1} and r_{μ_2} as the corresponding coefficients.

The excitation energy, being correct up to second-order, is obtained via the diagonalization of the following Hermitian Jacobian:

$$\mathbf{A}^{\text{ADC}(2)} = \begin{pmatrix} \frac{1}{2}(\langle \mu_1 | [[H, T_2], \tau_{v_1}] | 0 \rangle + \langle v_1 | [[H, T_2], \tau_{\mu_1}] | 0 \rangle) & \langle \mu_1 | [H, \tau_{v_2}] | 0 \rangle \\ \langle \mu_2 | [H, \tau_{v_1}] | 0 \rangle & \langle \mu_2 | [F, \tau_{v_2}] | 0 \rangle \end{pmatrix}, \quad (6)$$

where $|\mu_n\rangle$ stands for n -fold excited configurations and F is the Fock-operator. Similar to the case of linear-response second-order coupled-cluster singles and doubles (LR-CC2),¹⁹ in practice, the

$$\sigma = \mathbf{A}^{\text{ADC}(2)} \mathbf{r} = \omega_{\text{ADC}(2)} \mathbf{r} \quad (7)$$

eigenvalue problem is recast as a non-linear eigenvalue equation

$$\sigma(\omega_{\text{ADC}(2)}, \mathbf{r}_1) = \mathbf{A}^{\text{eff}}(\omega_{\text{ADC}(2)}) \mathbf{r}_1 = \omega_{\text{ADC}(2)} \mathbf{r}_1, \quad (8)$$

where $\omega_{\text{ADC}(2)}$ is the ADC(2) excitation energy and \mathbf{r}_1 (\mathbf{r}) is a vector composed of the r_{μ_1} (r_{μ_1} and r_{μ_2}) coefficients. The benefit is that the resulting equation with the effective Jacobian

matrix $\mathbf{A}^{\text{eff}}(\omega_{\text{ADC}(2)})$ has to be solved only for the r_{μ_1} amplitudes corresponding to single excitations. The elements of the effective Jacobian read explicitly as

$$A_{\mu_1 v_1}^{\text{eff}}(\omega_{\text{ADC}(2)}) = A_{\mu_1 v_1} - \sum_{\gamma_2} \frac{A_{\mu_1 \gamma_2} A_{\gamma_2 v_1}}{\varepsilon_{\gamma_2} - \omega_{\text{ADC}(2)}}, \quad (9)$$

with $\varepsilon_{\gamma_2} = -D_{ij}^{ab}$ if $\tau_{\gamma_2} = E_{ai} E_{bj}$.

In the following, we briefly collect the working equations required for the implementation of the ADC(2) method in spatial MO basis because, to the best of our knowledge, they are not published in the literature. Deriving the expressions corresponding to Eq. (8) we arrive at the

$$\begin{aligned} \sigma_{ia} = & \sum_{jb} [2(ia|jb) - (ij|ab)] r_j^b + (\varepsilon_a - \varepsilon_i) r_i^a + \frac{1}{2} \sum_{kjbc} [2(kc|jb) - (jc|kb)] r_k^c (2t_{ij}^{ab} - t_{ji}^{ab}) + \frac{1}{2} \sum_{kjbc} [2(ia|jb) - (ja|ib)] r_k^c (2t_{kj}^{cb} - t_{jk}^{cb}) \\ & + \frac{1}{2} \sum_{kjbc} (ib|ck) (2t_{jk}^{bc} - t_{kj}^{bc}) r_j^a + \frac{1}{2} \sum_{kjbc} (jb|ck) (2t_{ik}^{bc} - t_{ki}^{bc}) r_j^a - \frac{1}{2} \sum_{kjbc} (jb|ck) (2t_{jk}^{ac} - t_{kj}^{ac}) r_i^b - \frac{1}{2} \sum_{kjbc} (ja|ck) (2t_{jk}^{bc} - t_{kj}^{bc}) r_i^b \\ & + \sum_{bkc} (ab|ck) \hat{R}_{ik}^{bc} - \sum_{cjk} (ij|ck) \hat{R}_{jk}^{ac} \end{aligned} \quad (10)$$

sigma vector elements for singlet excitations, while for the triplet case the sigma vector reads as

$$\begin{aligned} \sigma_{ia} = & - \sum_{jb} (ij|ab) r_j^b + (\varepsilon_a - \varepsilon_i) r_i^a + \frac{1}{2} \sum_{kjbc} (jc|kb) r_k^c t_{ji}^{ab} + \frac{1}{2} \sum_{kjbc} (ja|ib) r_k^c t_{jk}^{cb} + \frac{1}{2} \sum_{kjbc} (ib|ck) (2t_{jk}^{bc} - t_{kj}^{bc}) r_j^a \\ & + \frac{1}{2} \sum_{kjbc} (jb|ck) (2t_{ik}^{bc} - t_{ki}^{bc}) r_j^a - \frac{1}{2} \sum_{kjbc} (jb|ck) (2t_{jk}^{ac} - t_{kj}^{ac}) r_i^b - \frac{1}{2} \sum_{kjbc} (ja|ck) (2t_{jk}^{bc} - t_{kj}^{bc}) r_i^b + \sum_{bkc} (ab|ck) \hat{R}_{ik}^{bc} - \sum_{cjk} (ij|ck) \hat{R}_{jk}^{ac}. \end{aligned} \quad (11)$$

The required \hat{R}_{μ_2} intermediates, having different expressions for the two different kinds of spin multiplicity, are defined in step 4 of the algorithm in Table I and are obtained using the

$$R_{\mu_2} = - \sum_{v_1} \frac{A_{\mu_2 v_1} r_{v_1}}{\varepsilon_{\mu_2} - \omega_{\text{ADC}(2)}} \quad (12)$$

amplitudes. The additional advantage of solving the rearranged pseudo-eigenvalue problem of Eq. (7) is that the R_{μ_2} amplitudes can be computed “on-the-fly” and their storage is not required.

Our implementation follows the ideas of Hättig and Weigend presented for their density-fitting LR-CC2 algo-

rithm.¹⁹ The main difference is that our working equations are written in the MO basis instead of the atomic orbital (AO) representation of Ref. 19 in order to efficiently utilize the reduced number of orbitals in the compressed NO basis. In the DF approach, the four-center two-electron integrals are approximated in a product form as

$$(pq|rs) = \sum_Q J_{pq}^Q J_{rs}^Q, \quad (13)$$

where capital indices, such as Q , denote the functions of the auxiliary basis set and the \mathbf{J} quantities are built from two- and three-center two-electron integrals, $(P|Q)$ and $(pq|P)$,

TABLE I. Algorithm and working equations for calculating the sigma vector for singlet and triplet excitations.

0. Perform MP2 calculation and store intermediate $Y_{ai}^Q = \sum_{jb} J_{jb}^Q (2t_{ij}^{ab} - t_{ji}^{ab})$
1. Calculate intermediates X^Q , X_{ij}^Q , and X_{ia}^Q
$X^Q = 2 \sum_{ia} J_{ia}^Q r_i^a$ $X_{ij}^Q = \sum_a J_{ia}^Q r_j^a$ $X_{ia}^Q = \sum_b r_i^b J_{ba}^Q$
2. Add purely r_i^a -dependent contributions to σ_{ia} and construct \bar{F}_{ia}
if singlet: $\sigma_{ia} \leftarrow \sum_Q J_{ia}^Q X^Q$
$\bar{F}_{ia} = -\sum_{jQ} J_{ja}^Q X_{ij}^Q + \sigma_{ia}$
if triplet: $\bar{F}_{ia} = \sum_{jQ} J_{ja}^Q X_{ij}^Q$
$\sigma_{ia} \leftarrow -\sum_{jQ} J_{ij}^Q X_{ja}^Q + (\varepsilon_a - \varepsilon_i) r_i^a$
3. Compute \hat{t}_{ij}^{ab} , add corresponding contributions to σ_{ia}
$(ia jb) = \sum_Q J_{ia}^Q J_{jb}^Q$
if singlet: $\hat{t}_{ij}^{ab} = [2(ia jb) - (ja ib)]/D_{ij}^{ab}$
if triplet: $\hat{t}_{ij}^{ab} = (ja ib)/D_{ij}^{ab}$
$\sigma_{ia} \leftarrow \frac{1}{2} \sum_{jb} \hat{t}_{ij}^{ab} \bar{F}_{jb}$
if singlet: $\sigma_{ia} \leftarrow \frac{1}{2} \sum_{jb} \sum_{kc} [2(ia jb) - (ja ib)] r_k^c \hat{t}_{jk}^{bc}$
if triplet: $\sigma_{ia} \leftarrow \frac{1}{2} \sum_{jb} \sum_{kc} (ja ib) r_k^c \hat{t}_{jk}^{bc}$
4. Construct the \bar{J}_{ia}^Q list, build intermediate \hat{R}_{ij}^{ab}
$\bar{J}_{ia}^Q = X_{ia}^Q - \sum_j J_{ij}^Q r_j^a$
$(\bar{ia} jb) = \sum_Q \bar{J}_{ia}^Q J_{jb}^Q$ $(ia \bar{jb}) = \sum_Q J_{ia}^Q \bar{J}_{jb}^Q$
if singlet: $\hat{R}_{ij}^{ab} = [2(\bar{ia} jb) - (\bar{ja} ib) + 2(ia \bar{jb}) - (ja \bar{ib})]/(D_{ij}^{ab} + \omega_{ADC(2)})$
$= (2\bar{R}_{ij}^{ab} - R_{ji}^{ab})/(D_{ij}^{ab} + \omega_{ADC(2)})$
if triplet: $\hat{R}_{ij}^{ab} = [2(\bar{ia} jb) - (\bar{ja} ib) - (ja \bar{ib})]/(D_{ij}^{ab} + \omega_{ADC(2)})$
$\bar{Y}_{ia}^Q = \sum_{jb} \hat{R}_{ij}^{ab} J_{jb}^Q$
5. Add the remaining contributions to σ_{ia}
$\sigma_{ia} \leftarrow \sum_{Qb} J_{ab}^Q \bar{Y}_{ib}^Q$
$\sigma_{ia} \leftarrow -\sum_{Qj} J_{ij}^Q \bar{Y}_{ja}^Q$
$\sigma_{ia} \leftarrow \frac{1}{2} \sum_j \sum_{Qb} (J_{ib}^Q Y_{jb}^Q + J_{jb}^Q Y_{ib}^Q) r_j^a$
$\sigma_{ia} \leftarrow -\frac{1}{2} \sum_b \sum_{Qj} (J_{jb}^Q Y_{ja}^Q + J_{ja}^Q Y_{jb}^Q) r_i^b$

respectively, as

$$J_{pq}^Q = \sum_P (pq|P)(P|Q)^{-1/2}. \quad (14)$$

The steps of the algorithm are given in detail in Table I. Inspecting the algorithm, one finds the construction of intermediates \hat{t}_{ij}^{ab} and \hat{R}_{ij}^{ab} (steps 3 and 4) from the three-center integrals and the contraction of the latter with the J_{jb}^Q list (step 4) as the rate-determining steps of the iterative process. The operation count for these steps is proportional to $n_{\text{occ}}^2 n_{\text{virt}}^2 n_{\text{aux}}$, where n_{occ} (n_{virt}) denotes the number of occupied (virtual) orbitals and n_{aux} stands for the number of auxiliary functions. Since the effective Jacobian, and thus σ as well, depends on the excitation energy, the non-linear eigenvalue problem cannot be solved simultaneously for all excited states. To solve the eigenvalue equations effectively, a procedure using a modified Davidson algorithm and the direct inversion in the iterative subspace (DIIS)⁸⁷ algorithm was implemented.^{19,86}

At the end of the iteration, the converged ADC(2) wave function is normalized, which is necessary for the evaluation of transition moments. To achieve this in spatial orbital basis, the amplitudes obtained are divided by the normalization

constant

$$c = \sqrt{\sum_{aibj} R_{ij}^{ab} R_{ij}^{ab} - \frac{1}{2} \sum_{aibj} R_{ij}^{ab} R_{ji}^{ab} + \sum_{ai} r_i^a r_i^a}. \quad (15)$$

Then the transition density matrix required for the ground to excited state transition moments can be obtained as

$$\begin{aligned} \rho_{pq} &= \langle \Psi^{\text{MP1}} | p^+ q^- | \Psi^{\text{ADC(2)}} \rangle \\ &= \langle 0 | (1 + T_2^\dagger) p^+ q^- (R_1 + R_2) (1 + T_2) | 0 \rangle \\ &= \langle 0 | p^+ q^- R_1 | 0 \rangle + \langle 0 | T_2^\dagger p^+ q^- R_1 | 0 \rangle \\ &\quad + \langle 0 | T_2^\dagger p^+ q^- R_1 T_2 | 0 \rangle + \langle 0 | T_2^\dagger p^+ q^- R_2 | 0 \rangle. \end{aligned} \quad (16)$$

This expression is often simplified^{88,89} by discarding disconnected contributions and by neglecting the higher than fifth-power scaling second-order terms. It can be shown that, analogous to LR-CC2, the resulting ADC(2) density matrix is consistent with the LR-CC theory and correct up to the first order. Our working equations for the transition density matrix in the spatial orbital basis are given for its various blocks by

$$\rho_{ab} = \sum_{ijc} R_{ij}^{ac} (2t_{ij}^{bc} - t_{ji}^{bc}), \quad (17)$$

$$\rho_{ij} = -\sum_{abk} R_{ik}^{ab} (2t_{jk}^{ab} - t_{kj}^{ab}), \quad (18)$$

$$\rho_{ai} = \sum_{bj} r_j^b (2t_{ij}^{ab} - t_{ji}^{ab}), \quad (19)$$

and

$$\begin{aligned} \rho_{ia} &= r_i^a - \sum_k r_k^a \sum_{cbj} t_{kj}^{cb} (2t_{ij}^{cb} - t_{ji}^{cb}) - \sum_c r_i^c \sum_{bjk} t_{kj}^{cb} (2t_{kj}^{ab} - t_{jk}^{ab}) \\ &= r_i^a - \sum_k r_k^a D_{ik}^{\text{MP2}} - \sum_c r_i^c D_{ac}^{\text{MP2}}, \end{aligned} \quad (20)$$

where D_{ik}^{MP2} and D_{ac}^{MP2} are the elements, respectively, of the occupied-occupied and the virtual-virtual block of the MP2 one-particle density matrix, and R_{ij}^{ab} of Eq. (12) is, in practice, built from the intermediates of step 4 of Table I as

$$R_{ij}^{ab} = \frac{(\bar{ia}|jb) + (ia|\bar{jb})}{D_{ij}^{ab} + \omega_{ADC(2)}}. \quad (21)$$

B. Construction of the reduced subspace

We have shown previously that, while preserving the intrinsic accuracy of the LR-CC2 excitation energies, the dimension of the virtual subspace can be significantly reduced by discarding NOs with low occupation numbers. On the other hand, the analogous frozen occupied NO approximation was found to be far less efficient for LR-CC2.⁸⁶ We experienced similar trends in the case of ADC(2), therefore we restrict the present discussion to the application of frozen virtual NOs. If they are of interest, the working equations required for the frozen occupied NO approximation can be obtained analogously.

First, the virtual-virtual block of the one-particle density matrix is constructed from a lower-level wave function Ψ ,

$$D_{ab} = \langle \Psi | a^+ b^- | \Psi \rangle. \quad (22)$$

The eigenvectors of this matrix are the virtual natural orbitals (VNOs), while its eigenvalues are interpreted as the corresponding occupation numbers of the VNOs. If Ψ is appropriately chosen, the NOs with smaller occupation numbers usually give a smaller contribution to the correlation or excitation energies. Therefore, in the frozen NO approximation, the NOs with occupation numbers below a predefined threshold, ε_{VNO} , are disregarded. The remaining VNOs will be denoted with a tilde (e.g., $\tilde{a}, \tilde{b}, \dots$), and the integral lists transformed to the VNO basis will also be distinguished with tildes (e.g., $\tilde{\mathbf{J}}$).

We have also demonstrated that the state-specific VNOs obtained from state-averaged density matrices are most suitable to efficiently compute LR-CC2 singlet excitation energies.⁸⁶ The state-averaged density matrix we have introduced is defined as $\mathbf{D} = (\mathbf{D}^{\text{MP2}} + \mathbf{D}^{\text{CIS(D)}})/2$, where \mathbf{D}^{MP2} and $\mathbf{D}^{\text{CIS(D)}}$ denote the density matrices obtained from the MP1 and the configuration interaction singles with perturbative doubles [CIS(D)] wave functions. The one-particle MP2 density matrix in a spatial orbital basis can be expressed in the form of

$$D_{ab}^{\text{MP2}} = \sum_{ijc} (2t_{ij}^{ca}t_{ij}^{cb} - t_{ij}^{ca}t_{ij}^{bc}). \quad (23)$$

The CIS(D) density matrix, $\mathbf{D}^{\text{CIS(D)}}$, is obtained as the sum of the density matrices derived from the CIS wave function and its second-order perturbative correction (D), $\mathbf{D}^{\text{CIS(D)}} = \mathbf{D}^{\text{CIS}} + \mathbf{D}^{(\text{D})}$. The CIS density matrix expressed in spatial orbitals reads as

$$D_{ab}^{\text{CIS}} = \sum_i c_i^a c_i^b \quad (24)$$

for both the singlet and the triplet states, where c_i^a is a CIS coefficient. The spin adaptation results in different expressions for matrix $\mathbf{D}^{(\text{D})}$ in the singlet and triplet cases. The expression for a singlet state is practically the same as for the MP2 density, Eq. (23), the only difference is that the MP2 amplitudes are substituted by the CIS(D) doubles coefficients. The latter can be expressed as

$$c_{ij}^{ab} = \frac{\sum_c [(ac|bj)c_i^c + (ai|bc)c_j^c] - \sum_k [(kj|ai)c_k^b + (ki|bj)c_k^a]}{D_{ij}^{ab} + \omega_{\text{CIS}}}, \quad (25)$$

where ω_{CIS} stands for the CIS excitation energy.^{90,91} For an excited state of triplet multiplicity, the virtual-virtual block of matrix $\mathbf{D}^{(\text{D})}$ is given as

$$D_{ab}^{(\text{D})} = \sum_{ijc} (\tilde{c}_{ij}^{ca}\tilde{c}_{ij}^{cb} + c_{ij}^{ca}c_{ij}^{cb} - c_{ij}^{ca}c_{ij}^{bc}), \quad (26)$$

where the c_{ij}^{ab} coefficients are still defined by Eq. (25), but they are built using the triplet CIS coefficients and excitation energy. Furthermore, \tilde{c}_{ij}^{ab} denotes the triplet-coupled CIS(D) doubles coefficient, which is evaluated as

$$\tilde{c}_{ij}^{ab} = \frac{\sum_c [(ac|bj)c_i^c - (ai|bc)c_j^c] + \sum_k [(kj|ai)c_k^b - (ki|bj)c_k^a]}{D_{ij}^{ab} + \omega_{\text{CIS}}}. \quad (27)$$

The algorithms and the working equations for the computation of the singlet density matrix were published previously.⁸⁶ The analogous steps and expressions for the triplet case are

TABLE II. Working equations for the evaluation of the triplet CIS(D) density matrix.

1. Add CIS contribution to the density matrix	$D_{ab}^{\text{CIS(D)}} \leftarrow \sum_i c_i^a c_i^b$
2. Compute intermediate Y_{ai}^Q	$Y_{ai}^Q \leftarrow \sum_c J_{ac}^Q c_i^c$
	$Y_{ai}^Q \leftarrow - \sum_j J_{ij}^Q c_j^a$
3. Compute intermediate V_{ij}^{ab}	$V_{ij}^{ab} = \sum_Q Y_{ai}^Q J_{bj}^Q$
4. Calculate c_{ij}^{ab} coefficients	$c_{ij}^{ab} = (V_{ij}^{ab} + V_{ji}^{ba})/(D_{ij}^{ab} + \omega_{\text{CIS}})$
5. Compute intermediate X_{ij}^{ab}	$X_{ij}^{ab} = c_{ij}^{ab} - c_{ij}^{ba}$
6. Add the first contribution to the density matrix	$D_{ab}^{\text{CIS(D)}} \leftarrow \sum_{ijc} c_{ij}^{ca} X_{ij}^{cb}$
7. Calculate \tilde{c}_{ij}^{ab} coefficients	$\tilde{c}_{ij}^{ab} = (V_{ij}^{ab} - V_{ji}^{ba})/(D_{ij}^{ab} + \omega_{\text{CIS}})$
8. Add the second contribution to the density matrix	$D_{ab}^{\text{CIS(D)}} \leftarrow \sum_{ijc} \tilde{c}_{ij}^{ca} \tilde{c}_{ij}^{cb}$

given in detail in Table II. Note that the one-particle MP2 density matrix is only constructed once, for the ground state. On the contrary, the CIS(D) wave function and hence the CIS(D) density matrix have to be evaluated for each excited state. The rate-determining step of the density matrix calculation, for both MP2 and CIS(D), is the assembly of the four-index integral list of intermediate \mathbf{V} (step 3), which is a fifth-power scaling operation with costs proportional to $n_{\text{occ}}^2 n_{\text{virt}}^2 n_{\text{aux}}$. The algorithm contains two additional fifth-power scaling operations (steps 6 and 8) with computational expenses proportional to $n_{\text{occ}}^2 n_{\text{virt}}^3$, while there is only one such term in the case of MP2 or singlet CIS(D).

In our previous LR-CC2 study, we have also introduced a simplification to the MP2 and (D) density matrices, with which the NO approximation works similarly well. Here we again take advantage of the neglect of the exchange-like terms from the corresponding density matrix expressions. With that approximation Eqs. (23) and (26) read, respectively, as

$$D_{ab}^{\text{MP2}} = \sum_{ijc} 2t_{ij}^{ca}t_{ij}^{cb} \quad (28)$$

and

$$D_{ab}^{(\text{D})} = \sum_{ijc} (\tilde{c}_{ij}^{ca}\tilde{c}_{ij}^{cb} + c_{ij}^{ca}c_{ij}^{cb}). \quad (29)$$

One benefit of this simplification is that the evaluation of intermediate X_{ij}^{ab} (step 5) can be omitted. In addition, the corresponding contribution to the density matrix can be obtained more efficiently via the multiplication of the CIS(D) doubles coefficient matrix with its transpose (step 6). On top of that, the implementation of the algorithm becomes significantly easier even if the entire integral lists or intermediates cannot be kept in the memory.

As expected, the VNOs constructed as described above are only ideal for ADC(2) calculations if CIS(D) is a good approximation to ADC(2). The prerequisite for this is that the CIS method provides a qualitatively good description of the excited state. If the coefficients of double excitations are not stored, a

good measure for the quality of the CIS and CIS(D) approximations is the overlap of the CIS and the single excitation part of the final ADC(2) wave functions. Our numerical experience shows that, if this overlap is relatively small, the ADC(2) calculations performed in the reduced VNO space may yield inadequate excitation energies and transition moments. In these cases, we found that the dominant excitations of the ADC(2) wave function obtained in the reduced space correspond to those of the CIS wave function, and particular excitations that have considerable weight in the canonical ADC(2) are missing. This problem cannot be resolved by tightening the ε_{VNO} threshold as the occupancy of the VNOs which do not noticeably contribute to the CIS wave function is rather low. To overcome this problem, we found the following approach to be useful.

In practice, for a particular excited state, the orbital energies of the canonical virtual orbitals contributing to the wave function are relatively close to each other. Thus, we can suppose that all the important orbitals will be included in the reduced space if it is augmented with the canonical virtual orbitals which are close in energy to the virtuals significantly contributing to the CIS wave function. For the selection of such orbitals, two further thresholds were introduced. First, those canonical virtual orbitals are chosen for which at least one CIS coefficient of an excitation involving them is greater than threshold ε_{CIS} . Second, all those canonical virtual orbitals are selected whose orbital energy is in a given interval. The lower limit of the interval is the orbital energy of the lowest MO selected in the first step minus threshold ε_E , while its upper limit is the orbital energy of the highest chosen MO plus ε_E . The orbitals of the reduced VNO space are projected out of the selected canonical virtual orbitals, and the remaining orbitals are orthonormalized employing canonical orthogonalization dropping the eigenvectors of the overlap matrix with eigenvalues lower than 10^{-7} . The resulting orthonormal MOs are added to the reduced VNO space, and the orbitals of the extended space are canonicalized. In practice, it means that the Fock-matrix is transformed to the extended MO space, and the matrix is diagonalized. The resulting pseudo-canonical orbitals and the corresponding orbital energies will be used in the subsequent calculations. For the sake of simplicity, from now on, this pseudo-canonical basis will be referred to as the VNO basis.

So far an accurate lower-rank approximation to the MP2 and ADC(2) wave functions has been introduced by defining the corresponding state-specific VNO basis. Analogously, the auxiliary basis can also be compressed by finding an appropriate basis transformation. It can be shown that the truncated singular vector basis of \mathbf{J} gives the most efficient approximation to \mathbf{J} itself and hence to the corresponding assembled four-center integrals.⁸⁵ In practice, it is more economical to obtain the singular vectors as the eigenvalues of matrix \mathbf{W} with elements

$$W_{PQ} = \sum_{pq} J_{pq}^P J_{pq}^Q. \quad (30)$$

Similar to the NO approach, the eigenvectors, the so-called NAFs, with eigenvalues below a predefined threshold, ε_{NAF} , are discarded in the compressed representation of \mathbf{J} .

In the following, we will employ two different sets of NAFs. First, as in our previous LR-CC2 study, we construct NAFs to compress the representation of the integrals in the NO basis. Here we build \mathbf{W} of Eq. (30) using $\hat{\mathbf{J}}$, the integral list transformed to the VNO basis. These NAFs will be referred to as restricted NO space NAFs or RS-NAFs for short. The RS-NAFs are suitable to reduce, for instance, the cost of certain assembly and σ -vector construction steps of the ADC(2) calculation (see, e.g., Table I). Another option is to utilize the NAF approximation right at the beginning, as soon as the three-center integrals are transformed to the canonical HF MO basis. These NAFs will be called the complete MO space NAFs, or shortly, CS-NAFs, and the corresponding \mathbf{J} integrals will be denoted hereafter by $\hat{\mathbf{J}}$. We note here that, naturally, the CS-NAF basis is usually significantly larger than the RS-NAF basis but still represents a compressed, system-specific auxiliary basis with which the expenses of the CIS calculation and density matrix evaluation steps can be cut roughly in half.

C. General algorithm

In this section, we briefly collect all the steps required for our reduced-cost ADC(2) algorithm. We introduce here two branches for test purposes in order to assess the accuracy of the CS-NAF approximation, which was not present in our previous study.⁸⁶ Algorithm 1 is basically the generalization of our VNO and (RS-)NAF approximation-based LR-CC2 scheme apart from the step that the VNOs selected using the ε_{VNO} threshold are supplemented with the close-lying canonical orbitals. This is extended in Algorithm 2 by the introduction of CS-NAFs as well (see step 2 below). Our general algorithm is as follows.

0. Solve HF equations
 1. Construct the canonical integral list \mathbf{J}
 2. If Algorithm 2: Calculate matrix \mathbf{W} using three-center integral list \mathbf{J} [Eq. (30)], and transform the auxiliary index of \mathbf{J} to the CS-NAF basis to obtain $\hat{\mathbf{J}}$
 3. Solve CIS equations for all the excited states simultaneously using either \mathbf{J} (Algorithm 1) or $\hat{\mathbf{J}}$ (Algorithm 2)
 4. Loop over excited states
 - 4.a. Calculate the state-averaged one-particle density matrix \mathbf{D} (Table II) using either \mathbf{J} (Algorithm 1) or $\hat{\mathbf{J}}$ (Algorithm 2), and construct the truncated virtual space. Transform the MO indices of \mathbf{J} or $\hat{\mathbf{J}}$ to the VNO basis to obtain $\bar{\mathbf{J}}$.
 - 4.b. Calculate matrix \mathbf{W} using three-index integrals $\bar{\mathbf{J}}$ [Eq. (30)], and transform the auxiliary index of $\bar{\mathbf{J}}$ to the RS-NAF basis ($\bar{\mathbf{J}}$). Write integral list $\bar{\mathbf{J}}$ to disk.
- End loop
5. Loop over excited states
 - 5.a. Retrieve integral list $\bar{\mathbf{J}}$ from disk
 - 5.b. Perform MP2 calculation and solve ADC(2) equations (Table I)
- End loop

We would like to point out that the CS-NAF approximation affects the accuracy of all the quantities computed

subsequently, such as density matrices, VNOs, and RS-NAFs. Besides that it is not guaranteed that the truncated RS-NAF basis of Algorithm 1 is a subset of the truncated CS-NAF basis even if the VNOs of the two algorithms can be considered the same in the case of a highly accurate CS-NAF approximation. In other words, if both NAF approximations are employed, contributions to the retained RS-NAFs coming from the dropped CS-NAFs are present in Algorithm 1, but they are lost in Algorithm 2. Both of these error sources will be extensively investigated in Sec. III.

III. RESULTS

A. Computational details

The presented reduced-cost ADC(2) algorithm has been implemented in the MRCC suite of quantum chemical programs and is available in the current release of the package.⁹²

For the benchmark calculations, Dunning’s correlation consistent basis sets augmented with diffuse functions (aug-cc-pVXZ, where $X = D, T, Q$) were used,^{93–95} and the corresponding auxiliary bases developed by Weigend *et al.* were employed in both the HF and the excited-state calculations.^{96–98} In the CIS and ADC(2) calculations, the core MOs were kept frozen.

To quantify the errors originating from our approximations, a test set of small molecules was employed containing examples for all important types of excitation.⁸⁶ Valence excitations ($n \rightarrow \pi^*$, $\pi \rightarrow \pi^*$, and $\sigma \rightarrow \pi^*$) are present among the transitions taken from the benchmark set of Thiel and co-workers.^{99,100} We have also added a couple of the Rydberg excited states of these systems to our test set as well as the CT excitations of an ethylene-tetrafluoroethylene system

(10 Å separation, taken from the work of Dreuw *et al.*¹⁰¹). We have also assessed the accuracy of our approach on a more realistic set of systems containing seven medium-sized, frequently studied molecules.^{86,102–110} Additional calculations were performed for even larger systems to demonstrate the efficiency of our implementation. For this purpose, molecules were taken from the studies of Grimme¹⁰³ and Schütz and co-workers.^{65–69} The systems included in the three sets are collected in Table III, while their structures are shown in the [supplementary material](#).

The reported computation times are wall-clock times determined on a machine equipped with 128 GB of main memory and a 6-core 3.5 GHz Intel Xeon E5-1650 processor.

B. Small molecules

First, we study the accuracy of our approximations on the example of the test set containing the smaller molecules. We analyze the accuracy of the singlet and triplet excitation energies as well as of the oscillator strengths corresponding to singlet transitions using the aug-cc-pVTZ basis set, which is probably the most relevant from the practical point of view; double- and quadruple- ζ -quality basis sets will be considered later. In order to find reliable default values for the VNO and NAF truncation thresholds, we rely on the results of our extensive convergence tests for ϵ_{VNO} and ϵ_{NAF} that we obtained for our related reduced-cost LR-CC2 scheme.⁸⁶ We found, with the default values of $\epsilon_{\text{VNO}} = 7.5 \times 10^{-5}$ and $\epsilon_{\text{NAF}} = 0.1$ a.u., the mean absolute error (MAE) of the singlet LR-CC2 excitation energies to be about 0.02 eV, which is an order of magnitude smaller than the intrinsic error of LR-CC2.^{111,112} Considering the close relation of the formulation of ADC(2) and LR-CC2,¹¹³ their comparable numerical

TABLE III. The size of the systems studied and the number of the basis functions in the basis sets considered.

Molecule	Number of atoms	Number of basis functions		
		aug-cc-pVDZ	aug-cc-pVTZ	aug-cc-pVQZ
Formaldehyde ^{99,100}	4	64	138	252
Formamide ^{99,100}	6	96	207	378
Acetamide ^{99,100}	9	137	299	550
Acetone ^{99,100}	10	146	322	596
Butadiene ^{99,100}	10	146	322	596
Benzene ^{99,100}	12	192	414	756
Ethylene-tetrafluoroethylene ¹⁰¹	12	220	460	824
Hydrazone dye ¹⁰⁵	21		828	
Diphenylamine ¹⁰⁵	21		851	
Azobenzene ¹⁰⁵	24		874	
6,6'-difluoro-indigo ^{102,103}	28		1150	
Bithiophene derivative ^{102,103}	29		1135	
<i>N</i> -methyl-2,3-benzocarbazole ^{102,103}	31		1127	
Flavone derivative ^{109,110}	36		1311	
Flv(a) ⁶⁶	51		2001	
Dyad ^{65,67,68}	53		2051	
Bisimide derivative ^{102,103}	60		2346	
Flv(b) ⁶⁶	78		2829	
D21L6 ^{68,69}	98		3412	

performance,^{36,64,108,114–116} and that our present scheme (especially Algorithm 1) employs similar considerations as our LR-CC2 method, the above default thresholds may seem appropriate for ADC(2) as well. However, the newly introduced elements of the algorithm require careful consideration. Accordingly, extensive benchmark calculations were carried out to study the size of the errors as a function of the various thresholds. The details can be found in the [supplementary material](#). On the basis of our numerical experience, the VNO and NAF thresholds have not been changed, while we propose $\varepsilon_{\text{CIS}} = 0.35$ and $\varepsilon_E = 0.15$ a.u. as the default thresholds for the virtual space completion. The errors of the approximate ADC(2) scheme for singlet excitation energies and the corresponding oscillator strengths (f) with respect to canonical ADC(2) are presented in Table IV using the default thresholds for both the VNO and NAF truncations. Looking at the results obtained with Algorithm 1, the MAE for singlet excitation energies in the small-molecule test set is 0.019 eV, while the maximum absolute error (MAX) is 0.040 eV. This accuracy is achieved by keeping only a fraction of the functions in the transformed bases, precisely, 52.6% of the VNOs and 81.6% of the RS-NAFs are dropped on the average. These mean values are quite representative; the fluctuation of the ratio of dropped VNOs and RS-NAFs for this test set is below 10% and 5%, respectively. The MAE of the excitation energies is less than that reported for singlet LR-CC2 excitations; however, the number of the VNOs and RS-NAFs is slightly larger⁸⁶ since the originally selected VNOs are augmented with the corresponding canonical orbitals. The errors for the corresponding

ADC(2) oscillator strengths are also highly acceptable being lower than 0.001 a.u. in average and below 0.005 a.u. in every case. If we compare the accuracy of Algorithm 2 (i.e., when CS-NAFs are also employed at the CIS iterations as well as at the VNO and RS-NAF construction steps) to that of Algorithm 1, we find its numerical performance just as good. There are only 2 meV and 1 meV differences in their MAE and MAX values, while the oscillator strengths are similarly accurate. This is explained by the fact that, except for a difference of less than 0.5%, the same portion of the VNOs and RS-NAFs is discarded by the two algorithms. The benefit of using Algorithm 2 over Algorithm 1 is that about 60% of the CS-NAFs can also be dropped without introducing any significant inaccuracy on top of that already present with Algorithm 1. Consequently, most of the steps preceding the ADC(2) calculation in the reduced VNO/RS-NAF basis can be performed about 60% faster with Algorithm 2.

To demonstrate the robustness of our approach, we have also studied the triplet excitations of the molecules of the same test set. The triplet excitations considered were selected so that their character and excited-state wave function (in terms of its dominant configurations) will be as close to the singlet excitations included in the test set as possible. Note that the oscillator strength is zero for the spin-forbidden transition from the singlet ground state to the triplet excited state; hence, oscillator strengths are not reported for the triplet excited states. The numerical values for the triplet excitation energies are collected in Table V. The MAE and MAX errors are somewhat larger than the corresponding values obtained for the singlet

TABLE IV. Canonical ADC(2) singlet excitation energies (ω , in eV), oscillator strength (f , in a.u.), the error of excitation energies ($\delta\omega$, in eV) and oscillator strengths (δf , in a.u.) with the present approach, and the percentage of VNOs and NAFs dropped using the default thresholds with the aug-cc-pVTZ basis set for small molecules. Oscillator strengths for symmetry-forbidden (s.f.) transitions are not displayed.

Molecule	State	Character	ω	f	$\delta\omega$	δf	Algorithm 1		$\delta\omega$	δf	Algorithm 2		
							Dropped VNOs	Dropped RS-NAFs			Dropped CS-NAFs	Dropped VNOs	Dropped RS-NAFs
Acetamide	S ₁	$n \rightarrow \pi^*$	5.356	0.000	0.005	0.000	53.7	82.3	0.006	0.000	59.3	54.1	82.6
	S ₂	Rydberg	5.869	0.018	0.017	0.000	53.7	81.5	0.018	0.000	59.3	54.1	82.1
	S ₃	Rydberg	6.450	0.012	0.028	0.000	51.6	81.0	0.028	0.000	59.3	51.6	81.7
Acetone	S ₁	$n \rightarrow \pi^*$	4.252	s.f.	0.011	s.f.	55.9	82.9	0.017	s.f.	60.1	56.2	83.1
	S ₁₄	$\sigma \rightarrow \pi^*$	8.959	0.000	0.009	0.000	55.6	82.9	0.012	0.000	60.1	55.6	83.0
	S ₁₆	$\pi \rightarrow \pi^*$	9.102	0.000	0.011	-0.005	55.6	82.9	0.015	-0.005	60.1	56.2	83.4
Benzene	S ₃	$\pi \rightarrow \pi^*$	6.507	s.f.	0.026	s.f.	55.5	83.7	0.026	s.f.	61.7	55.7	83.9
	S ₅	$\pi \rightarrow \pi^*$	7.041	0.069	0.029	0.000	56.0	83.7	0.033	0.000	61.7	57.0	84.0
Butadiene	S ₁	$\pi \rightarrow \pi^*$	6.095	0.707	-0.009	0.001	54.7	83.3	-0.009	0.000	61.4	55.7	83.9
	S ₅	$\pi \rightarrow \pi^*$	7.112	s.f.	0.009	s.f.	51.5	83.4	0.008	s.f.	61.4	52.1	83.4
Formaldehyde	S ₁	$n \rightarrow \pi^*$	3.834	s.f.	0.037	s.f.	48.5	79.3	0.036	s.f.	59.5	50.0	80.3
	S ₆	$\sigma \rightarrow \pi^*$	9.030	0.001	0.016	0.000	49.2	79.6	0.020	0.000	59.5	49.2	80.3
	S ₁₂	$\pi \rightarrow \pi^*$	10.557	0.038	0.026	0.000	46.9	79.9	0.025	0.000	59.5	46.9	79.9
Formamide	S ₃	Rydberg	6.688	0.015	0.028	0.000	49.7	79.6	0.027	0.000	59.0	49.7	80.0
C ₂ F ₄ → C ₂ H ₄	S ₁₇	CT	9.577	0.000	0.040	0.000	53.0	79.6	0.041	0.000	58.1	53.0	79.8
C ₂ H ₄ → C ₂ F ₄	S ₃₄	CT	10.915	0.000	0.006	0.000	50.5	79.2	0.008	0.000	58.1	46.5	79.3
Average					0.019 ^a	0.000 ^a	52.6	81.6	0.021 ^a	0.000 ^a	59.9	52.7	81.9
Maximum					0.040 ^b	0.005 ^b	56.0	83.7	0.041 ^b	0.005 ^b	61.7	57.0	84.0
Minimum					0.005 ^c	0.000 ^c	46.9	79.2	0.006 ^c	0.000 ^c	58.1	46.5	79.3

^aMAE.

^bMAX.

^cMinimum absolute error (MIN).

TABLE V. Canonical ADC(2) triplet excitation energies (ω , in eV), the error of excitation energies ($\delta\omega$, in eV) with the present approach, and the percentage of VNOs and NAFs dropped using the default thresholds with the aug-cc-pVTZ basis set for small molecules.

Molecule	State	Character	ω	Algorithm 1			Algorithm 2			
				$\delta\omega$	Dropped VNOs	Dropped RS-NAFs	$\delta\omega$	Dropped CS-NAFs	Dropped VNOs	Dropped RS-NAFs
Acetamide	T ₁	$n \rightarrow \pi^*$	5.099	0.017	50.2	80.9	0.019	59.3	50.5	81.3
	T ₂	Rydberg	5.831	0.029	55.8	81.5	0.030	59.3	55.8	82.6
	T ₄	Rydberg	6.298	0.035	54.1	80.9	0.034	59.3	54.1	81.7
Acetone	T ₁	$n \rightarrow \pi^*$	3.887	0.025	56.2	82.7	0.026	60.1	56.2	82.9
	T ₈	$\sigma \rightarrow \pi^*$	8.345	0.020	55.2	82.1	0.023	60.1	55.9	83.0
	T ₉	$\pi \rightarrow \pi^*$	8.999	0.033	54.6	82.3	0.034	60.1	54.6	82.7
Benzene	T ₅	$\pi \rightarrow \pi^*$	6.468	0.033	55.5	83.6	0.032	61.7	56.0	83.7
	T ₇	$\pi \rightarrow \pi^*$	6.986	0.038	56.5	83.4	0.038	61.7	57.0	83.8
Butadiene	T ₁	$\pi \rightarrow \pi^*$	3.434	0.027	55.7	83.3	0.027	61.4	55.7	83.3
	T ₈	$\pi \rightarrow \pi^*$	7.483	0.013	56.4	83.6	0.013	61.4	56.7	84.0
Formaldehyde	T ₁	$n \rightarrow \pi^*$	3.375	0.048	49.2	78.9	0.047	59.5	50.0	79.6
	T ₇	$\sigma \rightarrow \pi^*$	8.260	0.036	49.2	79.3	0.037	59.5	49.2	79.3
	T ₁₄	$\pi \rightarrow \pi^*$	10.506	0.022	46.2	79.6	0.022	59.5	46.2	79.6
Formamide	T ₃	Rydberg	6.159	0.037	52.8	80.9	0.038	59.0	52.8	81.1
C ₂ F ₄ \rightarrow C ₂ H ₄	T ₁₉	CT	9.573	0.040	53.0	79.5	0.041	58.1	53.0	79.7
C ₂ H ₄ \rightarrow C ₂ F ₄	T ₃₇	CT	10.913	0.007	50.2	78.9	0.005	58.1	50.9	79.4
Average				0.029 ^a	53.2	81.3	0.029 ^a	59.9	53.4	81.7
Maximum				0.048 ^b	56.2	83.6	0.047 ^b	61.7	57.0	84.0
Minimum				0.007 ^c	46.2	78.9	0.005 ^c	58.1	46.2	79.3

^aMAE.^bMAX.^cMIN.

excitations, but both values are more than appropriate. The comparable accuracy can be explained by the fact that the VNO and NAF approximations function almost identically in the two spin cases if the default thresholds are applied. Since we find the CS-NAF approximation similarly accurate for the triplet states as well, we simplify the rest of our numerical analysis by focusing on Algorithm 2 from this point. For the

sake of completeness, the corresponding data for Algorithm 1 are presented in the [supplementary material](#).

We also investigated the AO basis-set dependence of our approximations by comparing the results calculated with the aug-cc-pVTZ basis set to those obtained with aug-cc-pVDZ and aug-cc-pVQZ. The statistical measures for the corresponding errors are collected in Table VI, while the

TABLE VI. Error measures for the ADC(2) excitation energies ($\delta\omega$, in eV) and oscillator strengths (δf , in a.u.), and the average, maximum, and minimum percentage of VNOs and NAFs dropped using the default thresholds with various basis sets for small molecules.

		aug-cc-pVDZ		aug-cc-pVTZ		aug-cc-pVQZ	
		Singlet	Triplet	Singlet	Triplet	Singlet	Triplet
$\delta\omega$	MAE	0.045	0.039	0.021	0.029	0.064	0.080
	MAX	0.086	0.079	0.041	0.047	0.125	0.124
	MIN	0.013	0.000	0.006	0.005	0.002	0.034
δf	MAE	0.001	...	0.000	...	0.001	...
	MAX	0.008	...	0.005	...	0.008	...
	MIN	0.000	...	0.000	...	0.000	...
Dropped CS-NAFs	Avg.	76.5	76.5	59.9	59.9	45.8	45.8
	Max.	77.5	77.5	61.7	61.7	47.5	47.5
	Min.	75.9	75.9	58.1	58.1	44.7	44.7
Dropped VNOs	Avg.	18.3	17.2	52.7	53.4	73.1	73.2
	Max.	25.1	25.1	57.0	57.0	76.2	76.8
	Min.	9.6	7.1	46.5	46.2	70.5	70.5
Dropped RS-NAFs	Avg.	80.5	80.3	81.9	81.7	87.8	87.9
	Max.	82.5	82.5	84.0	84.0	89.1	89.8
	Min.	77.9	77.4	79.3	79.3	86.3	86.3

results for the individual molecules are given in Tables SIII–SVI of the [supplementary material](#). The MAE and MAX errors of the excitation energies with the aug-cc-pVDZ and aug-cc-pVQZ bases are about 2–3 times larger than the aug-cc-pVTZ errors. Not surprisingly, the same trend was observed for LR-CC2 in our previous study.⁸⁶ We find this acceptable because the errors are still significantly lower than the intrinsic error of the ADC(2) method. Moreover, usually at least a triple- ζ basis set augmented with diffuse functions is necessary to bring down the AO basis-set error to the level comparable to the intrinsic error of ADC(2) (or LR-CC2). In other words, double- ζ -quality basis sets are less relevant in production level calculations. On the other hand, the use of the quadruple- ζ -quality sets is often not economical or even impossible in practice. Additionally, the error of our approximations for the transition moments is fairly basis set independent.

Considering the basis-set dependence of the ratio of the retained VNOs and NAFs, we again find the similar trend observed previously for LR-CC2. Explicitly, the portion of the neglectable VNOs increases with the basis set size from 18% through 53% up to 73% for aug-cc-pVDZ, aug-cc-pVTZ, and aug-cc-pVQZ, respectively. As expected, larger basis sets can be compressed more when describing the same correlation effect. An opposite trend is present for the CS-NAFs, which is explained by the fact that the ratio of the functions in the AO and the corresponding auxiliary bases increases with the cardinal number, but the number of the AO product densities also increases, and a larger portion of the original auxiliary basis is required to be retained for their accurate fitting. Finally, after introducing the system-dependently compressed VNO and CS-NAF spaces, the percentage of the discarded RS-NAFs becomes nearly basis set independent. All in all, the operation count and data size reduction is sizeable with all the basis sets. For instance, the 53% VNO and the 82% RS-NAF reduction yield a 25-fold cut in the operation count in the rate-determining steps of the ADC(2) iteration as well as a 25-times smaller three-center integral list with the aug-cc-pVTZ basis. This gain is even larger, almost 120-fold with the aug-cc-pVQZ basis set.

C. Representative examples

We have also tested the accuracy of our approximations on larger systems to demonstrate that the errors do not grow with the system size. For that purpose, seven medium-sized dye molecules were collected from the literature (see the middle panel of Table III), which were also useful in realistic applications. Using the default truncation thresholds determined above, we computed the errors of singlet excitation energies and the corresponding oscillator strengths using Algorithm 2 with respect to conventional ADC(2) (see Table VII). Comparing the error measures with those obtained for the smaller molecules (see Table IV), we find a very good agreement. In fact, the MAE (MAX) of singlet excitation energies of the larger systems is even slightly better, being 0.015 (0.036) eV, than the corresponding value of 0.021 (0.041) eV presented in Table IV. We note that the oscillator strengths are more representative from the practical point of view than for the smaller

molecules because there is at least one large value (around 0.2 a.u.) for each molecule. However, the errors of the individual oscillator strengths are only moderately larger than those for the smaller test molecules; the quality of the approximate oscillator strengths and the simulated spectra is excellent. The MAE of the oscillator strengths is 0.002 a.u., but two salient errors can be found in the test set. For the S_1 state of diphenylamine and the S_7 state of the benzocarbazole derivative, the errors are -0.023 and 0.013 a.u., respectively. In both cases, the CIS wave function is a poor approximation for the corresponding ADC(2) wave function; nevertheless, the improved version of the reduced space construction algorithm results in acceptable errors.

The average portion of the dropped CS-NAFs, VNOs, and RS-NAFs, being about 60%, 56%, and 82%, respectively, does not decrease either; hence, similarly good or better speedups are expected in practice for these larger systems.

The above analysis is also performed for the seven lowest-lying triplet excitations on the same set of medium-sized dye molecules. If we first compare the errors obtained for the triplet excitations compiled in Table VIII to the corresponding singlet excitation energy errors in Table VII, we find that the triplet MAE is slightly smaller (0.009 vs. 0.015 eV), while the triplet MAX is a bit worse (0.042 vs. 0.036 eV), but both values are more than acceptable. A more noticeable difference, 0.009 vs. 0.029 eV, appears if the average triplet excitation energy error is compared to that for the smaller test molecules (see Table V). However, this is at least partly explained by the fact that the smaller-molecule test set is less balanced in terms of low- and high-lying excited states. Finally, looking at the portion of the omitted VNOs and NAFs, we find the former to be around 57% and the latter to be around 82% in average, which are very close to the corresponding values calculated for the smaller test systems. For the sake of completeness, we also mention that these findings hold not only for the results obtained with Algorithm 2 but with Algorithm 1 as well. The corresponding data for the singlet and triplet excitations are provided in Tables SVII and SVIII of the [supplementary material](#).

So far we have characterized the efficiency of our approximations by reporting the ratio of the omitted VNOs and NAFs and determining the expected operation count reduction at certain steps of the algorithm. An even better measure for that purpose is to compare the actual wall-clock times measured for the conventional and the reduced-cost ADC(2) variants. The total wall-clock times will be further partitioned into contributions required for the major steps of the computation. For the conventional approach, these parts include the time of the transformation of the three-center integrals from AO to canonical MO basis (t_J), and the time of the CIS (t_{CIS}) and the ADC(2) ($t_{\text{ADC}(2)}$) iterations. In the case of the reduced-cost algorithm, the overhead required for the evaluation and diagonalization of the necessary state-averaged density matrices and the \mathbf{W} matrices and the integral transformation to the VNO/NAF bases are accumulated into $t_{\bar{J}}$. On top of this, in the case of Algorithm 2, the time required for the construction of the CS-NAF basis ($t_{\text{CS-NAF}}$) and the corresponding integral transformation is added to t_J leading to $t_{\bar{J}} = t_J + t_{\text{CS-NAF}}$.

TABLE VII. Canonical ADC(2) singlet excitation energies (ω , in eV), oscillator strengths (f , in a.u.), the error of excitation energies ($\delta\omega$, in eV) and oscillator strengths (δf , in a.u.) with the present approach, and the percentage of VNOs and NAFs dropped using the default thresholds with the aug-cc-pVTZ basis set for medium-sized molecules. Oscillator strengths for symmetry-forbidden (s.f.) transitions are not displayed.

Molecule	State	Character	ω	$\delta\omega$	f	δf	Dropped CS-NAFs	Dropped VNOs	Dropped RS-NAFs
Hydrazone dye	S ₁	$\pi \rightarrow \pi^*$	3.475	-0.002	0.111	-0.001	58.7	54.1	80.4
	S ₂	CT	3.643	0.004	s.f.	s.f.	58.7	55.3	80.9
	S ₃	$n, \sigma \rightarrow \pi^*$	3.670	0.005	s.f.	s.f.	58.7	54.5	80.7
	S ₄	$\pi \rightarrow \pi^*$	4.073	-0.007	0.459	-0.004	58.7	53.4	80.3
	S ₅	$n, \sigma \rightarrow \pi^*$	4.268	0.006	0.000	0.000	58.7	54.5	80.7
	S ₆	$n, \sigma \rightarrow \pi^*$	4.287	0.006	0.001	0.000	58.7	55.2	80.9
	S ₇	$\pi \rightarrow \pi^*$	5.007	-0.026	0.050	-0.006	58.7	54.0	80.5
Azobenzene	S ₁	$n, \sigma \rightarrow \pi^*$	2.795	0.023	s.f.	s.f.	61.1	58.6	83.5
	S ₂	$\pi \rightarrow \pi^*$	4.064	-0.009	0.718	-0.005	61.1	57.1	83.0
	S ₃	$\pi \rightarrow \pi^*$	4.448	-0.019	0.020	-0.001	61.1	56.2	82.9
	S ₄	$\pi \rightarrow \pi^*$	4.455	-0.019	s.f.	s.f.	61.1	57.4	83.0
	S ₅	$\pi \rightarrow \pi^*$	5.182	-0.024	s.f.	s.f.	61.1	56.9	82.9
	S ₆	Rydberg	6.127	0.027	0.001	0.000	61.1	56.2	83.3
	S ₇	Rydberg	6.315	0.028	s.f.	s.f.	61.1	57.5	83.3
Diphenylamine	S ₁	$\pi \rightarrow \pi^*$	4.335	-0.011	0.104	-0.023	60.8	56.9	83.5
	S ₂	$\pi \rightarrow \pi^*$, Ryd.	4.418	-0.010	0.194	0.002	60.8	56.7	83.3
	S ₃	$\pi \rightarrow \pi^*$	4.460	-0.010	0.021	0.000	60.8	56.7	83.3
	S ₄	Rydberg	4.649	0.015	0.158	-0.008	60.8	56.6	83.3
	S ₅	Rydberg	5.045	0.027	0.049	-0.004	60.8	58.3	83.8
	S ₆	Rydberg	5.144	0.036	0.000	0.000	60.8	58.6	83.9
	S ₇	$\pi \rightarrow \pi^*$	5.275	0.027	0.003	0.000	60.8	58.1	83.8
6,6'-difluoro-indigo	S ₁	$n, \sigma \rightarrow \pi^*$	1.965	0.006	0.000	0.000	59.9	54.7	81.0
	S ₂	$n, \sigma \rightarrow \pi^*$	2.479	0.004	s.f.	s.f.	59.9	54.8	81.1
	S ₃	$\pi \rightarrow \pi^*$	2.933	-0.009	0.173	-0.003	59.9	55.8	81.2
	S ₄	$\pi \rightarrow \pi^*$	3.431	-0.010	s.f.	s.f.	59.9	54.6	81.0
	S ₅	$\pi \rightarrow \pi^*$	3.678	-0.018	s.f.	s.f.	59.9	54.4	80.9
	S ₆	$\pi \rightarrow \pi^*$	3.697	-0.017	0.140	0.000	59.9	54.4	80.9
	S ₇	$n, \sigma \rightarrow \pi^*$	3.748	-0.003	s.f.	s.f.	59.9	55.9	81.2
Bithiophene derivative	S ₁	$\pi \rightarrow \pi^*$	3.803	-0.017	0.588	0.000	60.7	55.3	82.3
	S ₂	$\pi \rightarrow \pi^*$	4.555	-0.016	0.012	-0.001	60.7	53.3	82.0
	S ₃	Rydberg	4.844	-0.004	0.000	0.000	60.7	55.3	82.2
	S ₄	$\pi \rightarrow \pi^*$	4.886	-0.022	0.041	-0.004	60.7	55.1	82.2
	S ₅	Rydberg	5.034	0.005	0.001	0.000	60.7	52.4	81.9
	S ₆	$n, \sigma \rightarrow \pi^*$	5.497	-0.003	0.001	0.000	60.7	52.4	81.9
	S ₇	$\pi \rightarrow \pi^*$	5.582	0.018	0.021	-0.006	60.7	55.0	82.3
N-methyl-2,3-benzocarbazole	S ₁	$\pi \rightarrow \pi^*$	3.304	-0.005	0.031	0.000	61.6	58.2	83.4
	S ₂	$\pi \rightarrow \pi^*$	4.057	-0.016	0.036	0.000	61.6	58.3	83.4
	S ₃	Rydberg	4.487	-0.015	0.310	-0.007	61.6	59.1	83.7
	S ₄	Rydberg	4.516	0.033	0.007	0.000	61.6	56.9	83.2
	S ₅	Rydberg	4.950	0.031	0.000	0.000	61.6	59.1	83.7
	S ₆	$\pi \rightarrow \pi^*$	5.027	0.031	0.105	0.000	61.6	59.1	83.7
	S ₇	Rydberg	5.271	-0.013	0.005	0.013	61.6	57.6	83.4
Flavone derivative	S ₁	CT	3.280	-0.009	0.616	-0.005	59.7	58.6	83.0
	S ₂	$\pi \rightarrow \pi^*$	3.922	-0.002	0.000	0.000	59.7	58.7	83.1
	S ₃	$n, \sigma \rightarrow \pi^*$	4.040	-0.016	0.065	0.000	59.7	58.7	83.1
	S ₄	$\pi \rightarrow \pi^*$	4.197	-0.004	0.014	0.000	59.7	56.9	82.9
	S ₅	Rydberg	4.398	0.030	0.015	0.000	59.7	59.1	83.2
	S ₆	$\pi \rightarrow \pi^*$	4.730	-0.020	0.030	0.009	59.7	58.2	82.9
	S ₇	Rydberg	4.869	0.024	0.001	0.000	59.7	59.0	83.2
Average				0.015 ^a		0.002 ^a	60.4	56.4	82.4
Maximum				0.036 ^b		0.023 ^b	61.6	59.1	83.9
Minimum				0.002 ^c		0.000 ^c	58.7	52.4	80.3

^aMAE.^bMAX.^cMIN.

TABLE VIII. Canonical ADC(2) triplet excitation energies (ω , in eV), the error of excitation energies ($\delta\omega$, in eV) with the present approach, and the percentage of VNOs and NAFs dropped using the default thresholds with the aug-cc-pVTZ basis set for small molecules.

Molecule	State	Character	ω	$\delta\omega$	Dropped CS-NAFs	Dropped VNOs	Dropped RS-NAFs
Hydrazone dye	T ₁	$\pi \rightarrow \pi^*$	3.161	0.009	58.7	54.4	80.5
	T ₂	CT	3.427	0.011	58.7	55.3	80.9
	T ₃	$\pi \rightarrow \pi^*$	3.447	0.012	58.7	54.5	80.7
	T ₄	$\pi \rightarrow \pi^*$	3.751	-0.002	58.7	54.1	80.5
	T ₅	$\pi \rightarrow \pi^*$	3.792	0.004	58.7	54.5	80.7
	T ₆	CT	4.189	0.004	58.7	54.8	80.7
	T ₇	$\pi \rightarrow \pi^*$	4.279	0.013	58.7	54.5	80.7
Azobenzene	T ₁	$n, \sigma \rightarrow \pi^*$	2.189	0.036	61.1	53.8	82.7
	T ₂	$\pi \rightarrow \pi^*$	2.879	0.014	61.1	58.0	83.2
	T ₃	$\pi \rightarrow \pi^*$	4.004	0.011	61.1	57.7	83.1
	T ₄	$\pi \rightarrow \pi^*$	4.241	-0.004	61.1	57.5	83.1
	T ₅	$\pi \rightarrow \pi^*$	4.302	-0.002	61.1	57.5	83.1
	T ₆	$\pi \rightarrow \pi^*$	4.712	0.011	61.1	56.4	83.0
	T ₇	$\pi \rightarrow \pi^*$	4.827	0.004	61.1	56.2	82.9
Diphenylamine	T ₁	$\pi \rightarrow \pi^*$	3.634	0.012	60.8	57.6	83.4
	T ₂	$\pi \rightarrow \pi^*$	4.103	0.008	60.8	57.1	83.3
	T ₃	$\pi \rightarrow \pi^*$	4.110	0.003	60.8	59.2	83.7
	T ₄	$\pi \rightarrow \pi^*$	4.263	0.009	60.8	57.2	83.4
	T ₅	Rydberg	4.531	0.042	60.8	58.8	83.8
	T ₆	$\pi \rightarrow \pi^*$	4.729	0.005	60.8	56.9	83.2
	T ₇	$\pi \rightarrow \pi^*$	4.817	0.002	60.8	57.3	83.4
6,6'-difluoro-indigo	T ₁	$\pi \rightarrow \pi^*$	2.087	0.011	59.9	56.0	81.2
	T ₂	$\pi \rightarrow \pi^*$	2.786	0.006	59.9	54.6	80.9
	T ₃	$\pi \rightarrow \pi^*$	3.286	-0.003	59.9	54.5	80.9
	T ₄	$\pi \rightarrow \pi^*$	3.448	0.001	59.9	54.6	81.0
	T ₅	$\pi \rightarrow \pi^*$	4.212	0.002	59.9	52.9	80.8
	T ₆	$\pi \rightarrow \pi^*$	4.292	-0.010	59.9	55.7	81.1
	T ₇	$\pi \rightarrow \pi^*$	4.357	0.002	59.9	52.9	80.7
Bithiophene derivative	T ₁	$\pi \rightarrow \pi^*$	2.697	0.011	61.6	55.4	82.2
	T ₂	$\pi \rightarrow \pi^*$	3.863	0.011	61.6	53.6	82.0
	T ₃	$\pi \rightarrow \pi^*$	4.013	0.009	61.6	55.5	82.3
	T ₄	$\pi \rightarrow \pi^*$	4.301	0.007	61.6	53.7	82.1
	T ₅	Rydberg	4.784	0.004	61.6	55.4	81.9
	T ₆	$\pi \rightarrow \pi^*$	5.262	-0.001	61.6	52.1	82.1
	T ₇	$n, \sigma \rightarrow \pi^*$	5.380	-0.005	61.6	55.2	82.2
N-methyl-2,3-benzocarbazole	T ₁	$\pi \rightarrow \pi^*$	2.703	0.011	60.7	58.7	83.5
	T ₂	$\pi \rightarrow \pi^*$	3.487	0.004	60.7	58.5	83.5
	T ₃	$\pi \rightarrow \pi^*$	3.764	0.003	60.7	58.4	83.4
	T ₄	$\pi \rightarrow \pi^*$	4.100	0.006	60.7	58.4	83.4
	T ₅	$\pi \rightarrow \pi^*$	4.379	-0.020	60.7	59.5	83.5
	T ₆	$\pi \rightarrow \pi^*$	4.489	0.008	60.7	59.1	83.7
	T ₇	$\pi \rightarrow \pi^*$	4.604	-0.009	60.7	59.6	83.7
Flavone derivative	T ₁	CT	2.585	0.010	59.7	59.0	83.1
	T ₂	$n, \sigma \rightarrow \pi^*$	3.537	0.002	59.7	59.0	83.1
	T ₃	$\pi \rightarrow \pi^*$	3.940	0.011	59.7	59.0	83.1
	T ₄	$n, \sigma \rightarrow \pi^*$	4.007	0.004	59.7	58.8	82.9
	T ₅	$\pi \rightarrow \pi^*$	4.277	-0.008	59.7	57.1	82.8
	T ₆	$\pi \rightarrow \pi^*$	4.650	0.001	59.7	57.2	82.9
	T ₇	$\pi \rightarrow \pi^*$	4.738	0.035	59.7	59.0	83.1
Average				0.009 ^a	60.4	56.5	82.4
Maximum				0.042 ^b	61.6	59.6	83.8
Minimum				0.001 ^c	58.7	52.1	80.5

^aMAE.^bMAX.^cMIN.

TABLE IX. The wall-clock times required for the various steps of the calculations in minutes.

Molecule	Canonical				Algorithm 2					Speedup
	$t_{\mathbf{J}}$	t_{CIS}	$t_{\text{ADC}(2)}$	t_{Total}	$t_{\mathbf{J}}$	t_{CIS}	$t_{\hat{\mathbf{J}}}$	$t_{\text{ADC}(2)}$	t_{Total}	
Azobenzene	6.2	4.4	352.6	363.1	6.5	1.7	6.7	19.7	34.6	10.5
Hydrazone dye	4.9	3.8	492.8	501.5	5.1	1.5	7.6	35.9	50.1	10.0
Diphenylamine	5.6	3.2	511.8	520.5	6.0	1.3	6.2	20.4	33.9	15.4
Benzocarbazole derivative	16.9	10.2	2218.1	2245.2	18.0	4.2	20.3	97.7	140.2	16.0
Indigo derivative	17.3	10.9	2032.4	2060.5	18.2	4.2	31.9	125.3	179.6	11.5
Bithiophene derivative	16.8	13.7	2894.5	2925.0	17.9	5.1	30.8	185.7	239.6	12.2
Flavone derivative	29.8	19.1	4926.7	4975.6	31.7	7.5	47.9	201.8	288.9	17.2
Average										13.3
Maximum										17.2
Minimum										10.0

Our wall-clock time measurements for the lowest-lying seven singlet and seven triplet excitation energies and the corresponding singlet transition moments of the seven medium-sized test molecules discussed previously are presented in Table IX for Algorithm 2. The analogous wall-clock times with Algorithm 1 are given in Table SIX of the [supplementary material](#). Most importantly, the average overall speedup factor with Algorithm 2 compared to the conventional algorithm is about 13 using the same hardware. This significant efficiency increase occurs quite reliably considering that the maximum (minimum) overall speedup is 17.2 (10.0). It can be seen that the time required for the CIS iterations as well as for the construction of VNOs and RS-NAFs can be halved compared to Algorithm 1 (cf. Table SIX of the [supplementary material](#)), while the additional computation cost needed for the construction of the CS-NAF basis with respect to the evaluation of the canonical integral list \mathbf{J} is only about 5%. Consequently, the total calculation can be performed about 25% faster (and with considerably reduced storage requirement) via Algorithm 2. We expect similar benefits from the introduction of CS-NAFs in our reduced-cost LR-CC2 method.⁸⁶

To demonstrate the potential of our approach, we determined the excitation energies and oscillator strengths for even larger molecules containing up to 98 atoms using the aug-cc-pVTZ basis set. Such extensive ADC(2) calculations with more than 3400 AOs are prohibitive or at least highly challenging with the conventional ADC(2) implementations. The calculated excited-state properties are collected in Table X for Algorithm 2, while Table SX of the [supplementary material](#) contains the analogous data for Algorithm 1. Again, the numerical result for the excitation energies and oscillator strengths computed with the two algorithms agree within a few thousandths of an eV and a.u., respectively. The characters and the energies of the studied singlet excitations match the ones obtained previously with our reduced-cost LR-CC2 method.⁸⁶ The percentage of the dropped VNOs and RS-NAFs lies again in the previously experienced regions at around 60% and 83%, respectively. Since these five systems cover a sizable range containing 51–98 atoms and 2001–3412 AOs, it seems normal that we observe a slight shift in the ratio of the omitted basis functions when going towards the larger systems. This

increase is, however, only about 6% for the VNOs and 2% for the RS-NAFs and can at least partially be attributed to the increasing quasi-redundancy in the augmented triple- ζ AO basis of these extended molecules. We also present in Table X the measured wall-clock times for the most demanding operations using Algorithm 2. Compared to the results of the measurements performed for the medium-sized systems, these timings are affected by the fact that neither the complete canonical integral list \mathbf{J} nor its CS-NAF compressed $\hat{\mathbf{J}}$ variant fits into the memory. For such cases, we also implemented the out-of-core versions of the necessary operations where the entire integral list is stored on the hard disk, and only blocks of suitable size are processed at a time. The use of the out-of-core algorithms is only required until the integral transformation to the VNO/RS-NAF bases is complete, for the ADC(2) iterations our scheme benefits from the greatly reduced data sizes in the compressed MO/auxiliary function spaces.

Looking at the wall-clock times, we can conclude that a single CIS iteration takes somewhat smaller time for the triplet states. This result is not surprising since the calculation of the Coulomb-term is not necessary. However, as it can be inferred from Table II, the construction of the triplet CIS(D) density matrix requires more operations; hence, $t_{\hat{\mathbf{J}}}$ is about 20% more expensive for the triplet states. An ADC(2) iteration takes slightly less time for the singlet states although it requires somewhat more operations. However, a couple of rate-determining steps (see in Table I) can be implemented more efficiently for singlet excitations. Compared to the ADC(2) excitation energy computation, the cost of the transition moments is almost negligible, taking only the time of roughly 1.2 iterations. If we compare the performance of the two algorithms (cf. Table X and Table SX of the [supplementary material](#)), we observe a small increase (from 5% to 20%) in the overhead required for the CS-NAF construction. This is explained by the disk I/O demand of the out-of-core CS-NAF algorithm not present previously. This cost increase is, however, amply compensated by the about 50% percent more economical CIS iteration and VNO as well as RS-NAF construction of Algorithm 2. In principle, the expenses of the ADC(2) iterations are independent of the choice of the auxiliary basis used for the VNO density matrix construction

TABLE X. ADC(2) excitation energies (ω , in eV) and oscillator strengths (f , in a.u.) computed with the present approach, the percentage of VNOs and NAFs dropped, and computation times (in min) using the default thresholds with the aug-cc-pVTZ basis set for the largest molecules.

Molecule	State	Character	ω	f	Dropped CS-NAFs	Dropped VNOs	Dropped RS-NAFs	$t_{\mathbf{j}}$	$t_{\text{CIS}}^{\text{a}}$	$t_{\mathbf{J}}^{\text{b}}$	$t_{\text{ADC}(2)}^{\text{c}}$	t_f^{d}
Flv(a)	S ₁	$\pi \rightarrow \pi^*$	2.601	0.303	59.2	58.1	82.2	226.3	1.4	34.8	4.0	5.3
	S ₂	$\pi \rightarrow \pi^*$	2.868	0.187	59.2	58.1	82.1			34.8	4.1	5.1
	S ₃	$n, \sigma \rightarrow \pi^*$	3.309	0.001	59.2	58.4	82.2			34.8	3.7	5.0
	S ₄	$\pi \rightarrow \pi^*$	3.511	0.112	59.2	58.1	82.2			34.8	3.7	5.0
	T ₁	$\pi \rightarrow \pi^*$	1.870	...	59.2	58.3	82.2		1.1	43.6	4.7	...
	T ₂	$\pi \rightarrow \pi^*$	2.367	...	59.2	58.3	82.1			43.5	4.5	...
	T ₃	CT	3.241	...	59.2	58.1	82.1			43.5	4.7	...
	T ₄	$\pi \rightarrow \pi^*$	3.602	...	59.2	58.3	82.1			43.4	4.5	...
Dyad	S ₁	$\pi \rightarrow \pi^*$	2.944	0.169	59.8	58.3	82.8	254.7	1.4	35.8	4.4	4.9
	S ₂	CT	3.314	0.001	59.8	58.6	82.9			35.9	4.3	4.8
	S ₃	$\pi \rightarrow \pi^*$	3.486	0.142	59.8	56.4	82.5			35.8	4.8	5.4
	S ₄	CT	3.790	0.045	59.8	58.1	82.8			35.8	4.3	4.8
	T ₁	$\pi \rightarrow \pi^*$	2.447	...	59.8	58.4	82.8		1.1	45.0	4.3	...
	T ₂	CT	3.010	...	59.8	56.6	82.5			45.2	5.0	...
	T ₃	CT	3.342	...	59.8	58.3	82.8			45.3	4.6	...
	T ₄	$\pi \rightarrow \pi^*$	3.701	...	59.8	58.2	82.7			45.1	4.5	...
Bisimide derivative	S ₁	$\pi \rightarrow \pi^*$	2.481	0.683	58.3	59.7	82.7	375.3	7.8	71.1	8.4	9.3
	S ₂	$\pi \rightarrow \pi^*$	3.434	0.000	58.3	59.8	82.8			71.1	7.9	9.3
	S ₃	$\pi \rightarrow \pi^*$	3.690	0.021	58.3	59.8	82.8			71.1	7.9	9.3
	S ₄	$\pi \rightarrow \pi^*$	3.782	0.000	58.3	57.3	82.5			71.1	8.6	9.9
	T ₁	$\pi \rightarrow \pi^*$	1.600	...	58.3	59.8	82.7		7.7	87.3	8.4	...
	T ₂	$\pi \rightarrow \pi^*$	2.993	...	58.3	57.6	82.5			87.2	9.8	...
	T ₃	$\pi \rightarrow \pi^*$	3.079	...	58.3	57.5	82.5			87.2	9.4	...
	T ₄	CT	4.267	...	58.3	60.1	82.9			87.3	8.3	...
Flv(b)	S ₁	$\pi \rightarrow \pi^*$	2.431	0.368	57.9	60.7	83.3	835.8	22.7	166.8	17.4	20.2
	S ₂	$\pi \rightarrow \pi^*$	2.847	0.169	57.9	61.5	83.4			166.8	16.4	19.1
	S ₃	$n, \sigma \rightarrow \pi^*$	3.219	0.148	57.9	60.8	83.3			166.7	16.9	19.7
	S ₄	$\pi \rightarrow \pi^*$	3.267	0.000	57.9	61.6	83.5			166.7	16.5	19.0
	T ₁	$\pi \rightarrow \pi^*$	1.741	...	57.9	60.9	83.3		16.8	203.4	15.7	...
	T ₂	$\pi \rightarrow \pi^*$	2.353	...	57.9	61.6	83.5			203.3	16.9	...
	T ₃	$\pi \rightarrow \pi^*$	2.727	...	57.9	61.0	83.4			203.4	17.9	...
	T ₄	$\pi \rightarrow \pi^*$	4.078	...	57.9	61.6	83.5			203.3	17.7	...
D21L6	S ₁	CT	2.600	1.056	59.0	61.9	84.4	1468.3	38.0	370.6	38.6	40.3
	S ₂	$\pi \rightarrow \pi^*$	3.368	0.109	59.0	60.6	84.2			370.7	39.3	42.2
	S ₃	Rydberg	3.464	0.061	59.0	61.6	84.3			370.7	37.6	41.6
	S ₄	Rydberg	4.044	0.019	59.0	61.5	84.3			370.8	37.6	41.3
	T ₁	CT	1.972	...	59.0	62.0	84.4		25.2	455.5	37.1	...
	T ₂	$\pi \rightarrow \pi^*$	2.601	...	59.0	61.9	84.4			455.7	38.0	...
	T ₃	$\pi \rightarrow \pi^*$	3.253	...	59.0	61.7	84.3			455.6	37.9	...
	T ₄	CT	3.482	...	59.0	61.9	84.3			455.9	37.5	...
Average					58.8	59.6	83.1					
Maximum					59.8	62.0	84.4					
Minimum					57.9	56.4	82.1					

^a Average wall-clock time for a CIS iteration using a multi-state algorithm.

^b Average wall-clock time for the construction of the $\bar{\mathbf{J}}$ integral list. The calculation of the MP2 density is distributed equally among the excited states.

^c Average wall-clock time for an ADC(2) iteration.

^d Wall-clock time required for the oscillator strength calculation.

(i.e., conventional vs. CS-NAF). As expected, in practice, we only see a negligible difference due to the fact that the size of the VNO and RS-NAF bases with Algorithms 1 and 2 are not completely identical but are very similar.

IV. CONCLUSIONS

An improved version of our virtual natural orbital and natural auxiliary function-based approximation⁸⁶ has been

presented, and the approach has been extended to the evaluation of triplet excitation energies and ground to excited state transition moments. In contrast to our previous approach, in the modified scheme the NAF approximation is invoked right at the beginning of the calculation, and the originally selected VNOs are supplemented with canonical orbitals. With the improved algorithm, we have significantly reduced the computation time required for the solution of the CIS equations and the construction of the VNOs and NAFs

necessary for the correlated excited-state calculations, which were among the rate-determining steps previously. Furthermore, the augmented reduced subspace considerably improves the robustness of the method and the accuracy of the computed properties.

We have derived and implemented the required working equations for the triplet CIS(D) density matrix and set up the infrastructure for the calculation of triplet excitation energies. The efficiency of the approximation has been demonstrated for the ADC(2) method, which is currently one of the most promising low-scaling correlated approaches for excited-state properties. We have implemented the working equations for ADC(2) singlet and triplet excitation energies as well as transition moments in the framework of our reduced-cost scheme.

Extensive benchmark calculations have been performed for singlet and triplet excitation energies as well as oscillator strengths for a representative test set including excitations of all the important types. On the basis of the results obtained, it can be stated that the average errors in the singlet and triplet excitation energies (0.02 eV) are an order of magnitude smaller than the error of the ADC(2) method. The maximum absolute error in the computed oscillator strengths does not exceed 0.025 a.u., while the mean absolute error is 0.002 a.u. The percentage of the neglected VNOs and NAFs seems to be constant independently of the size of the system for any type of excitation. With these approximations, an average speedup of more than an order of magnitude can be achieved for ADC(2) calculations. Our results also demonstrate that, using the new approach, the excited states of extended systems including up to 100 atoms can be routinely studied with reliable basis sets at the ADC(2) level.

SUPPLEMENTARY MATERIAL

See [supplementary material](#) for molecular structures, excitation energies, and oscillator strengths computed with various algorithms and basis sets.

ACKNOWLEDGMENTS

The authors are thankful to Professor Andreas Köhn for helpful discussions regarding the implementation of the transition densities. The authors are grateful for the financial support from the National Research, Development, and Innovation Office (NKFIH, Grant No. KKP126451). The work of P.R.N. is supported through the New National Excellence Program of the Ministry of Human Capacities, ID: ÚNKP-17-4-BME-55. The computing time granted on the Hungarian HPC Infrastructure at NIIF Institute, Hungary, is gratefully acknowledged.

¹M. E. Casida, "Recent advances in density functional methods," in *Computational Chemistry: Reviews of Current Trends*, edited by D. P. Chong (World Scientific, Singapore, 1999), Vol. 1.

²M. E. Casida and M. Huix-Rotllant, *Annu. Rev. Phys. Chem.* **63**, 287 (2012).

³J. Ridley and M. Zerner, *Theor. Chim. Acta* **32**, 111 (1973).

⁴M. C. Zerner, G. H. Loew, R. F. Kirchner, and U. T. Mueller-Westerhof, *J. Am. Chem. Soc.* **102**, 589 (1980).

⁵W. Weber and W. Thiel, *Theor. Chem. Acc.* **103**, 495 (2000).

⁶A. Koslowski, M. E. Beck, and W. Thiel, *J. Comput. Chem.* **24**(6), 714 (2003).

⁷J. F. Stanton and R. J. Bartlett, *J. Chem. Phys.* **98**, 7029 (1993).

⁸J. D. Watts and R. J. Bartlett, *J. Chem. Phys.* **101**, 3073 (1994).

⁹H. Koch and P. Jørgensen, *J. Chem. Phys.* **93**, 3333 (1990).

¹⁰H. Koch, H. J. A. Jensen, P. Jørgensen, and T. Helgaker, *J. Chem. Phys.* **93**, 3345 (1990).

¹¹R. J. Rico and M. Head-Gordon, *Chem. Phys. Lett.* **213**, 224 (1993).

¹²J. Čížek, *J. Chem. Phys.* **45**, 4256 (1966).

¹³J. Oddershede, *Adv. Quantum Chem.* **11**, 275 (1978).

¹⁴J. Oddershede, *Adv. Chem. Phys.* **69**, 201 (1987).

¹⁵B. O. Roos, P. R. Taylor, and P. E. M. Siegbahn, *Chem. Phys.* **48**, 157 (1980).

¹⁶O. Christiansen, H. Koch, and P. Jørgensen, *Chem. Phys. Lett.* **243**, 409 (1995).

¹⁷O. Christiansen, H. Koch, P. Jørgensen, and T. Helgaker, *Chem. Phys. Lett.* **263**, 530 (1996).

¹⁸K. Hald, C. Hättig, D. L. Yeager, and P. Jørgensen, *Chem. Phys. Lett.* **328**, 291 (2000).

¹⁹C. Hättig and F. Weigend, *J. Chem. Phys.* **113**, 5154 (2000).

²⁰C. Hättig, *J. Chem. Phys.* **118**, 7751 (2003).

²¹A. Köhn and C. Hättig, *J. Chem. Phys.* **119**, 5021 (2003).

²²J. Oddershede and P. Jørgensen, *J. Chem. Phys.* **66**, 1541 (1977).

²³E. S. Nielsen and P. Jørgensen, *J. Chem. Phys.* **73**, 6238 (1980).

²⁴J. Oddershede, P. Jørgensen, and D. L. Yeager, *Comput. Phys. Rep.* **2**, 33 (1984).

²⁵J. Schirmer, *Phys. Rev. A* **26**, 2395 (1982).

²⁶A. B. Trofimov, G. Stelter, and J. Schirmer, *J. Chem. Phys.* **111**, 9982 (1999).

²⁷A. B. Trofimov, G. Stelter, and J. Schirmer, *J. Chem. Phys.* **117**, 6402 (2002).

²⁸S. Grimme and M. Parac, *ChemPhysChem* **4**, 292 (2003).

²⁹A. Dreuw and M. Head-Gordon, *Chem. Rev.* **105**, 4009 (2005).

³⁰T. Helgaker, P. Jørgensen, and J. Olsen, *Molecular Electronic Structure Theory* (Wiley, Chichester, 2000).

³¹R. J. Buenker and S. D. Peyerimhoff, *Theor. Chim. Acta* **35**, 33 (1974).

³²J. Schirmer, *Phys. Rev. A* **43**, 4647 (1991).

³³F. Mertins and J. Schirmer, *Phys. Rev. A* **53**, 2140 (1996).

³⁴J. Schirmer and A. B. Trofimov, *J. Chem. Phys.* **120**, 11449 (2004).

³⁵J. H. Starcke, M. Wormit, and A. Dreuw, *J. Chem. Phys.* **130**, 024104 (2009).

³⁶P. H. P. Harbach, M. Wormit, and A. Dreuw, *J. Chem. Phys.* **141**, 064113 (2014).

³⁷M. Wormit, D. R. Rehn, P. H. P. Harbach, J. Wenzel, C. M. Krauter, E. Epifanovsky, and A. Dreuw, *Mol. Phys.* **112**, 774 (2014).

³⁸M. Wormit and A. Dreuw, *Wiley Interdiscip. Rev.: Comput. Mol. Sci.* **5**, 82 (2015).

³⁹C. M. Krauter, M. Pernpointner, and A. Dreuw, *J. Chem. Phys.* **138**, 044107 (2013).

⁴⁰S. Knippenberg, D. R. Rehn, M. Wormit, J. H. Starcke, I. L. Rusakova, A. B. Trofimov, and A. Dreuw, *J. Chem. Phys.* **136**, 064107 (2012).

⁴¹T. Fransson, D. R. Rehn, A. Dreuw, and P. Norman, *J. Chem. Phys.* **146**, 094301 (2017).

⁴²J. Wenzel, A. Holzer, M. Wormit, and A. Dreuw, *J. Chem. Phys.* **142**, 214104 (2015).

⁴³S. Mai, F. Plasser, M. Pabst, F. Neese, A. Köhn, and L. González, *J. Chem. Phys.* **147**, 184109 (2017).

⁴⁴D. Lefrancois, M. Wormit, and A. Dreuw, *J. Chem. Phys.* **143**, 124107 (2015).

⁴⁵S. Prager, A. Zech, F. Aquilante, A. Dreuw, and T. A. Wesolowski, *J. Chem. Phys.* **144**, 204103 (2016).

⁴⁶S. F. Boys, G. B. Cook, C. M. Reeves, and I. Shavitt, *Nature* **178**, 1207 (1956).

⁴⁷J. L. Whitten, *J. Chem. Phys.* **58**, 4496 (1973).

⁴⁸B. I. Dunlap, J. W. D. Connolly, and J. R. Sabin, *J. Chem. Phys.* **71**, 3396 (1979).

⁴⁹M. Feyereisen, G. Fitzgerald, and A. Komornicki, *Chem. Phys. Lett.* **208**, 359 (1993).

⁵⁰N. O. C. Winter and C. Hättig, *J. Chem. Phys.* **134**, 184101 (2011).

⁵¹E. G. Hohenstein, R. M. Parrish, and T. J. Martínez, *J. Chem. Phys.* **137**, 044103 (2012).

⁵²R. M. Parrish, E. G. Hohenstein, T. J. Martínez, and C. D. Sherrill, *J. Chem. Phys.* **137**, 224106 (2012).

- ⁵³E. G. Hohenstein, R. M. Parrish, C. D. Sherrill, and T. J. Martínez, *J. Chem. Phys.* **137**, 221101 (2012).
- ⁵⁴E. G. Hohenstein, S. I. L. Kakkila, R. M. Parrish, and T. J. Martínez, *J. Chem. Phys.* **138**, 124111 (2013).
- ⁵⁵E. G. Hohenstein, S. I. L. Kakkila, R. M. Parrish, and T. J. Martínez, *J. Phys. Chem. B* **117**, 12972 (2013).
- ⁵⁶R. Send, V. R. I. Kaila, and D. Sundholm, *J. Chem. Phys.* **134**, 214114 (2011).
- ⁵⁷R. Send, C.-M. Suomivuori, V. R. I. Kaila, and D. Sundholm, *J. Phys. Chem. B* **119**, 2933 (2015).
- ⁵⁸A. P. Gamiz-Hernandez, I. N. Angelova, R. Send, D. Sundholm, and V. R. I. Kaila, *Angew. Chem., Int. Ed.* **54**, 11564 (2015).
- ⁵⁹C.-M. Suomivuori, N. O. C. Winter, C. Hättig, D. Sundholm, and V. R. I. Kaila, *J. Chem. Theory Comput.* **12**, 2644 (2016).
- ⁶⁰C. Yang and A. Dreuw, *J. Comput. Chem.* **38**, 1528 (2017).
- ⁶¹P. Pulay, *Chem. Phys. Lett.* **100**, 151 (1983).
- ⁶²P. Pulay and S. Saebø, *Theor. Chim. Acta* **69**, 357 (1986).
- ⁶³M. Schütz, *J. Chem. Phys.* **142**, 214103 (2015).
- ⁶⁴B. Helmich and C. Hättig, *Comput. Theor. Chem.* **1040-1041**, 35 (2014).
- ⁶⁵D. Kats, T. Korona, and M. Schütz, *J. Chem. Phys.* **125**, 104106 (2006).
- ⁶⁶D. Kats, T. Korona, and M. Schütz, *J. Chem. Phys.* **127**, 064107 (2007).
- ⁶⁷D. Kats and M. Schütz, *J. Chem. Phys.* **131**, 124117 (2009).
- ⁶⁸K. Freundorfer, D. Kats, T. Korona, and M. Schütz, *J. Chem. Phys.* **133**, 244110 (2010).
- ⁶⁹K. Ledermüller, D. Kats, and M. Schütz, *J. Chem. Phys.* **139**, 084111 (2013).
- ⁷⁰K. Ledermüller and M. Schütz, *J. Chem. Phys.* **140**, 164113 (2014).
- ⁷¹P. Baudin and K. Kristensen, *J. Chem. Phys.* **144**, 224106 (2016).
- ⁷²P. Baudin and K. Kristensen, *J. Chem. Phys.* **146**, 214114 (2017).
- ⁷³W. Meyer, *J. Chem. Phys.* **58**, 1017 (1973).
- ⁷⁴P. J. Hay, *J. Chem. Phys.* **59**, 2468 (1973).
- ⁷⁵R. Ahlrichs, H. Lischka, V. Staemmler, and W. Kutzelnigg, *J. Chem. Phys.* **62**, 1225 (1975).
- ⁷⁶A. G. Taube and R. J. Bartlett, *J. Chem. Phys.* **128**, 164101 (2008).
- ⁷⁷A. E. DePrince and C. D. Sherrill, *J. Chem. Theory Comput.* **9**, 293 (2013).
- ⁷⁸Z. Rolik and M. Kállay, *J. Chem. Phys.* **134**, 124111 (2011).
- ⁷⁹Z. Rolik, L. Szegedy, I. Ladjánszki, B. Ladóczki, and M. Kállay, *J. Chem. Phys.* **139**, 094105 (2013).
- ⁸⁰A. Landau, K. Khistyayev, S. Dolgikh, and A. I. Krylov, *J. Chem. Phys.* **132**, 014109 (2010).
- ⁸¹A. Kumar and T. D. Crawford, *J. Phys. Chem. A* **121**, 708 (2017).
- ⁸²R. Flores-Moreno and J. V. Ortiz, *J. Chem. Phys.* **128**, 164105 (2008).
- ⁸³O. Dolgounitcheva, R. Flores-Moreno, V. G. Zakrzewski, and J. V. Ortiz, *Int. J. Quantum Chem.* **108**, 2862 (2008).
- ⁸⁴V. G. Zakrzewski, O. Dolgounitcheva, A. V. Zakjevskii, and J. V. Ortiz, *Annu. Rep. Comput. Chem.* **6**, 79 (2010).
- ⁸⁵M. Kállay, *J. Chem. Phys.* **141**, 244113 (2014).
- ⁸⁶D. Mester, P. R. Nagy, and M. Kállay, *J. Chem. Phys.* **146**, 194102 (2017).
- ⁸⁷P. Pulay, *Chem. Phys. Lett.* **73**, 393 (1980).
- ⁸⁸B. Lunkenheimer and A. Köhn, *J. Chem. Theory Comput.* **9**, 977 (2013).
- ⁸⁹M. Pabst and A. Köhn, *J. Chem. Phys.* **129**, 214101 (2008).
- ⁹⁰M. Head-Gordon, R. J. Rico, M. Oumi, and T. J. Lee, *Chem. Phys. Lett.* **219**, 21 (1994).
- ⁹¹G. E. Scuseria, A. C. Scheiner, T. J. Lee, J. E. Rice, and H. F. Schaefer III, *J. Chem. Phys.* **86**, 2881 (1987).
- ⁹²M. Kállay, Z. Rolik, J. Csontos, P. Nagy, G. Samu, D. Mester, J. Csóka, I. Ladjánszki, L. Szegedy, B. Ladóczki, K. Petrov, M. Farkas, and B. Hégyel, MRCC, a quantum chemical program suite, see also Ref. ⁷⁹ as well as <http://www.mrcc.hu/>.
- ⁹³T. H. Dunning, Jr., *J. Chem. Phys.* **90**, 1007 (1989).
- ⁹⁴R. A. Kendall, T. H. Dunning, Jr., and R. J. Harrison, *J. Chem. Phys.* **96**, 6796 (1992).
- ⁹⁵D. E. Woon and T. H. Dunning, Jr., *J. Chem. Phys.* **98**, 1358 (1993).
- ⁹⁶F. Weigend, A. Köhn, and C. Hättig, *J. Chem. Phys.* **116**, 3175 (2002).
- ⁹⁷F. Weigend, M. Häser, H. Patzelt, and R. Ahlrichs, *Chem. Phys. Lett.* **294**, 143 (1998).
- ⁹⁸F. Weigend, *J. Comput. Chem.* **29**, 167 (2008).
- ⁹⁹M. Schreiber, M. R. Silva-Junior, S. P. A. Sauer, and W. Thiel, *J. Chem. Phys.* **128**, 134110 (2008).
- ¹⁰⁰M. R. Silva-Junior, S. P. A. Sauer, M. Schreiber, and W. Thiel, *Mol. Phys.* **108**, 453 (2010).
- ¹⁰¹A. Dreuw, J. L. Weisman, and M. Head-Gordon, *J. Chem. Phys.* **119**, 2943 (2003).
- ¹⁰²M. Parac and S. Grimme, *J. Phys. Chem. A* **106**, 6844 (2002).
- ¹⁰³L. Goerigk, J. Moellmann, and S. Grimme, *Phys. Chem. Chem. Phys.* **11**, 4611 (2009).
- ¹⁰⁴L. Goerigk and S. Grimme, *J. Chem. Phys.* **132**, 184103 (2010).
- ¹⁰⁵A. Matsuura, H. Sato, W. Sotoyama, A. Takahashi, and M. Sakurai, *J. Mol. Struct.: THEOCHEM* **860**, 119 (2008).
- ¹⁰⁶D. Jacquemin, V. Wathelet, E. A. Perpète, and C. Adamo, *J. Chem. Theory Comput.* **5**, 2420 (2009).
- ¹⁰⁷D. Jacquemin, E. A. Perpète, I. Ciofini, C. Adamo, R. Valero, Y. Zhao, and D. G. Truhlar, *J. Chem. Theory Comput.* **6**, 2071 (2010).
- ¹⁰⁸D. Jacquemin, I. Duchemin, and X. Blase, *J. Chem. Theory Comput.* **11**, 5340 (2015).
- ¹⁰⁹D. A. Yushchenko, O. B. Vadzyuk, S. O. Kosterin, G. Duportail, Y. Mély, and V. G. Pivovarenko, *Anal. Biochem.* **369**, 218 (2007).
- ¹¹⁰C. A. Kenfack, A. S. Klymchenko, G. Duportail, A. Burgerc, and Y. Mély, *Phys. Chem. Chem. Phys.* **14**, 8910 (2012).
- ¹¹¹O. Christiansen, H. Koch, P. Jørgensen, and J. Olsen, *Chem. Phys. Lett.* **256**, 185 (1996).
- ¹¹²H. Koch, O. Christiansen, P. Jørgensen, and J. Olsen, *Chem. Phys. Lett.* **244**, 75 (1995).
- ¹¹³C. Hättig, *Adv. Quantum Chem.* **50**, 37 (2015).
- ¹¹⁴N. O. C. Winter, N. K. Graf, S. Leutwyler, and C. Hättig, *Phys. Chem. Chem. Phys.* **15**, 6623 (2013).
- ¹¹⁵R. Send, M. Kühn, and F. Furche, *J. Chem. Theory Comput.* **7**, 2376 (2011).
- ¹¹⁶S. Budzák, G. Scalmani, and D. Jacquemin, *J. Chem. Theory Comput.* **13**, 6237 (2017).